Paleogeodetic records of seismic and aseismic subduction from central Sumatran microatolls, Indonesia

Danny Hilman Natawidjaja,[1,2] Kerry Sieh,[1] Steven N. Ward,[3] Hai Cheng,[4] R. Lawrence Edwards,[4] John Galetzka,[1,5] and Bambang W. Suwargadi[6]

[1]   We utilize coral microatolls in western Sumatra to document vertical deformation associated with subduction. Microatolls are very sensitive to fluctuations in sea level and thus act as natural tide gauges. They record not only the magnitude of vertical deformation associated with earthquakes (paleoseismic data), but also continuously track the long-term aseismic deformation that occurs during the intervals between earthquakes (paleogeodetic data). This paper focuses on the twentieth century paleogeodetic history of the equatorial region. Our coral paleogeodetic record of the 1935 event reveals a classical example of deformations produced by seismic rupture of a shallow subduction interface. The site closest to the trench rose 90 cm, whereas sites further east sank by as much as 35 cm. Our model reproduces these paleogeodetic data with a 2.3 m slip event on the interface 88 to 125 km from the trench axis. Our coral paleogeodetic data reveal slow submergence during the decades before and after the event in the areas of coseismic emergence. Likewise, interseismic emergence occurred before and after the 1935 event in areas of coseismic submergence. Among the interesting phenomenon we have discovered in the coral record is evidence of a large aseismic slip or "silent event" in 1962, 27 years after the 1935 event. Paleogeodetic deformation rates in the decades before, after, and between the 1935 and 1962 events have varied both temporally and spatially. During the 25 years following the 1935 event, submergence rates were dramatically greater than in prior decades. During the past four decades, however, rates have been lower than in the preceding decades, but are still higher than they were prior to 1935. These paleogeodetic records enable us to model the kinematics of the subduction interface throughout the twentieth century.   *INDEX TERMS:* 1206 Geodesy and Gravity: Crustal movements—interplate (8155); 7215 Seismology: Earthquake parameters; 7221 Seismology: Paleoseismology; 7223 Seismology: Seismic hazard assessment and prediction; 8107 Tectonophysics: Continental neotectonics; *KEYWORDS:* paleoseismology, paleogeodesy, coral microatoll, earthquake cycle, elastic model

1.   Introduction

1.1.   Motivation

[2]   Understanding the sequential rupture of active faults or earthquake cycles is a fundamental unrealized goal in earthquake science. Common outstanding questions concern the regularity of fault rupture, repeatability of the pattern of slip on a fault, and the roles of geologic structure and rheology in governing ruptures. Clearly, answers to these and related questions are essential to progress in both the practical and academic realms of earthquake science. A key reason for slow progress is that relevant data bearing on how strains accumulate in the blocks surrounding faults and how faults release accumulated strains are very limited and are difficult to obtain. Well-documented seismic histories that extend through more than one earthquake cycle are uncommon. *Thatcher* [1989], for example, found only 12 large fault segments in the Circum-Pacific region for which the record was relatively complete for the past single earthquake cycle. For subduction earthquakes, evidence is particularly sparse, because the seismic sources crop out under water.

[3]   Paleoseismology has contributed to obtaining evidence of serial fault ruptures. However, progress has been

---

[1]Division of Geological and Planetary Sciences, California Institute of Technology, Pasadena, California, USA.
[2]Now at Research Center for Geotechnology, Indonesian Institute of Sciences, Bandung, Indonesia.
[3]Institute of Geophysics and Planetary Physics, University of California, Santa Cruz, California, USA.
[4]Department of Geology and Geophysics, University of Minnesota, Minneapolis, Minnesota, USA.
[5]Formerly at U.S. Geological Survey, Pasadena, California, USA.
[6]Research Center for Geotechnology, Indonesian Institute of Sciences, Bandung, Indonesia.

hampered by the imprecision and incompleteness of most records and by the difficulty of data acquisition. Data sets longer than one earthquake cycle are rare and generally incomplete and imprecise [*Sieh*, 1996]. Even where excellent geological evidence or well documented histories of past events exist, for example, along the San Andreas Fault [*Sieh et al.*, 1989], the Cascadian subduction zone [*Atwater*, 1992], and the Nankai subduction zone [*Ando*, 1975; *Kanamori*, 1973], data on strain accumulation throughout the interseismic periods is largely lacking. This is because, unlike earthquake events that produce large, nearly instantaneous signals across a narrow fault zone, interseismic deformation accrues over tens, hundreds, or even thousands of years and tens of kilometers of crust. To gather preinstrumental evidence of these slow deformations we need a very stable and long-lived natural recorder.

[4] The validity and utility of theoretical models can be rigorously examined only if long and detailed records of large earthquakes are available. A thousand years hence, modern geodetic and seismologic instrumental records will likely have provided most of the requisite data. In the meantime, however, there will be a pressing need to collect paleoseismologic and paleogeodetic records for clues to the long-term behavior of faults.

[5] This challenge motivated us to investigate the use of coral "microatolls" on fringing reefs above the Sumatran subduction interface. Microatolls not only record the magnitude of vertical deformation associated with earthquakes (paleoseismic data) [*Taylor et al.*, 1987], but their long lives and great sensitivity enable them also to continuously track slow aseismic, interseismic deformation (paleogeodetic data) [*Sieh et al.*, 1999; *Zachariasen*, 1998; *Zachariasen et al.*, 2000]. Furthermore, coral microatolls are abundant on the islands off the west coast of Sumatra, only 70 to 150 km inland from the trench axis, and thus, are ideally located above the locked part of the subduction interface.

[6] These outer-arc islands, composed primarily of deformed accretionary prism sediments and coralline limestone, are the sub-aerial expression of the crest of the outer-arc rise [*Budhitrisna and Andi Mangga*, 1990]. There has been little, if any, net vertical displacement of the islands in the Holocene epoch, because all of the mid-Holocene microatolls found in the islands between 3°S and the equator (Figure 1) are less than 2 m above their modern counterparts [*Zachariasen et al.*, 1999]. Models of Holocene global isostatic adjustment to deglaciation indicate sea level in this area reached a maximum of about 2 to 3 m above the present level about 5000 years ago [*Peltier and Tushingham*, 1991; *Zachariasen et al.*, 1999]. Thus the motions we document are elastic deformations associated with the cyclic accumulation and relief of strain.

1.2. Coral Microatoll as Paleoseismic and Paleogeodetic Recorder

[7] Massive corals act as stable, long-lived, natural recorders of sea level changes with sensitivities of about 1 cm [*Sieh et al.*, 1999; *Taylor et al.*, 1987; *Zachariasen et al.*, 1999, 2000]. They enable examination of sea level time series that extend back well before periods of instrumental record. Massive corals or coral heads grow on shallow reefs on warm, low-latitude coasts. The microatoll morphologies form because the upward growth of corals heads is limited

by lowest tide levels, above which exposure causes death [*Sieh et al.*, 1999; *Taylor et al.*, 1987; *Zachariasen et al.*, 1999, 2000]. This uppermost limit to coral growth has been called "the highest level of survival" ("HLS"). Therefore fluctuations in sea level or HLS are accurately imprinted on the morphology and stratigraphy of microatolls. In west Sumatra, the HLS history recovered from corals is associated predominantly with crustal deformation above the subduction interface.

[8] Coral growth typically shows annual pairs of dark and light bands. This annual banding is caused by seasonal variations in the density of the coral skeletons [*Knutson and Smith*, 1972; *Scoffin and Stoddart*, 1978; *Taylor et al.*, 1987; *Zachariasen et al.*, 1999, 2000]. The light, lower density bands grow during the rainy season (September to March), and the dark band, higher density bands form during the dry season (April–August). These annual bands are similar to tree rings in that they provide a yearly record of coral growth throughout the life of the coral, and thus provide an excellent time series for constructing sea level history. The annual bands are sometimes visible to the naked eye, but are more pronounced in x-radiographs of thin slabs, cut parallel to the direction of coral growth.

[9] To establish HLS time series at a site, we mapped the intertidal reef, documented the height, shape and dimensions of many of the coral heads, and collected slab samples from the heads that were representative of the overall population. We employed a hand-held GPS receiver with an accuracy of about 10 m for coarser and broader mapping and an electronic total station with accuracy of a few millimeters or better for high-resolution mapping. We collected samples with a hydraulic chainsaw designed for underwater use. We surveyed the upper surfaces of the sampled microatolls prior to the cutting and the removal of the slabs, so that we could later determine the elevation of any part on the slab relative to points on other microatolls and the surrounding environment. At a few sites, our colleagues, M. Gagan and N. Abrams of Australian National University (ANU), took drill cores from coral heads. The primary purpose of their sampling was to investigate paleoclimatic changes, but they also helped us constrain the ages of the fossil heads.

[10] Usually, we were able to sample from sites where our slabs represented a large population of coral heads displaying a similar history. We avoided collecting from microatolls whose HLS history might not reflect open-ocean sea level [*Scoffin and Stoddart*, 1978]. Our detailed topographic surveys of the reef substrate told us if during lowest tides water on the intertidal reef flat would be ponded at the outer edge of the shallow reef flat. Thus we were able to ensure that the recovered sea level history from collected samples reflected that of the open sea. We collected samples from microatolls that were unaffected by local tilting or subsidence. Such disturbances are relatively easy to recognize, either by visual inspection in the field or by anomalous elevations relative to other heads at the site.

1.3. Tectonics of the Active Sumatran Plate Boundary

[11] Along the west coast of Sumatra, the Australian and Indian oceanic plates are subducting obliquely at rates that range from about 50 to 70 mm/yr beneath the SE Asian plate (Figure 1). The plate convergence largely partitions
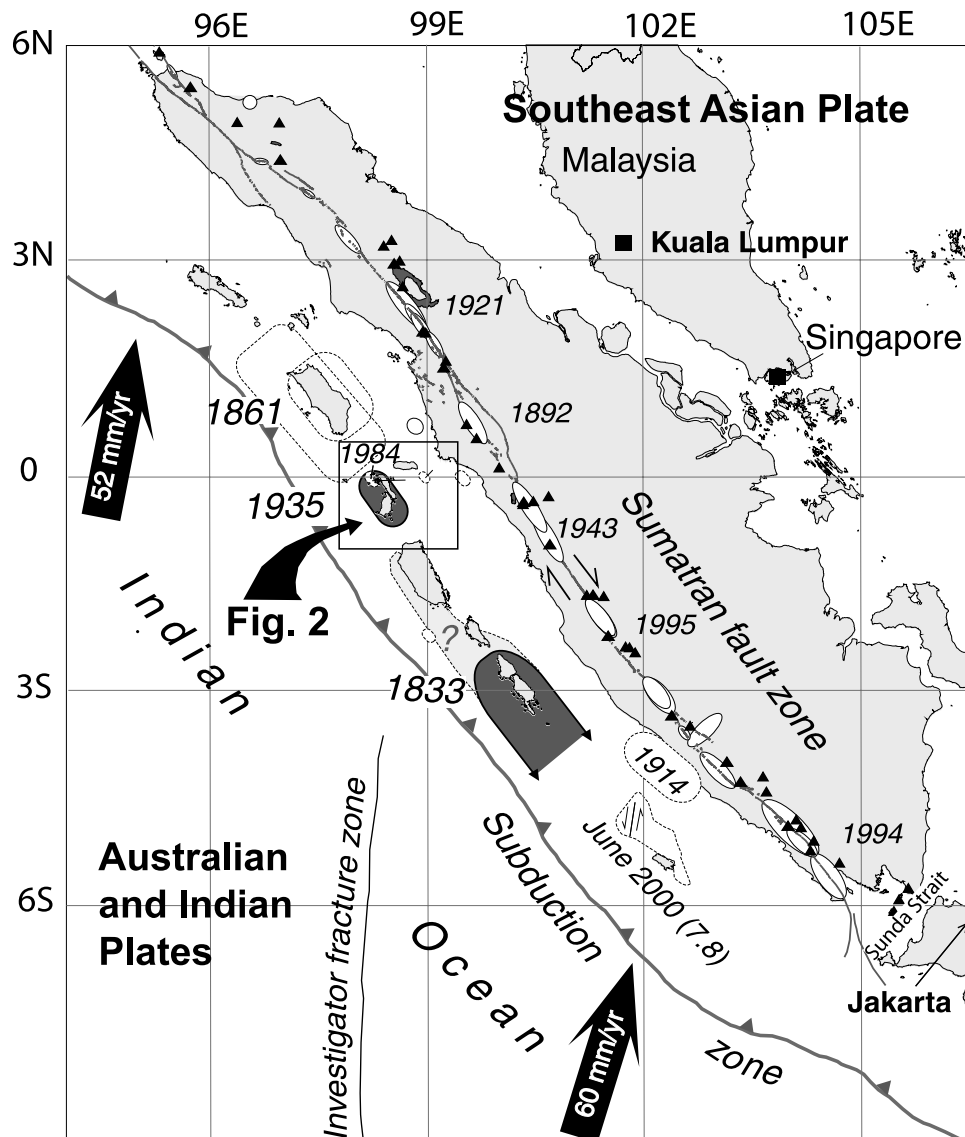
Figure 1. Map of major structural elements and seismicity of Sumatran plate boundary. Oblique subduction of the Indian and Australia plates beneath Sumatra is accommodated principally by slip on the Sumatran subduction zone and the dextral Sumatran fault. Triangles are active volcanoes. Arrows are plate motions from GPS [*Prawirodirdjo*, 2000]. Source regions of large earthquakes from historical and seismographic records and are in white ellipses. Those augmented from coral microatoll study appear as dark-shaded ellipses. This study presents paleoseismic and paleogeodetic time series from coral heads, decades to centuries long in the vicinity of the equator.

into a frontal dip-slip component that is accommodated by slip on the subduction interface and a right-lateral strike-slip component that is mostly accommodated by the Sumatran fault [*Fitch*, 1972; *Katili and Hehuwat*, 1967; *McCaffrey*, 1991; *Sieh and Natawidjaja*, 2000; *Sieh et al.*, 2000].

[12] The Sumatran subduction zone accommodates most of the plate convergence [*McCaffrey*, 1991]. Two very large earthquakes, a $M \sim 9$ in the 1833 and a $M \sim 8.5$ in 1861, dominate the historical seismicity of the subduction interface (Figure 1). Historical records of shaking and tsunamis suggest that these two events involved rupture of all or most of the interface between about 2°N and 5°S [*Newcomb and McCann*, 1987]. In the equatorial region, however, the principal event for the last century is the M 7.7 earthquake

of 1935 [*Rivera et al.*, 2002]. This earthquake also involved rupture of a part of the subduction interface, sandwiched in between the sources of the 1861 and the 1833 ruptures (Figure 1). Figure 2 shows the instrumental record of smaller earthquake over the twentieth century.

[13] The M_w 7.9 of June 2000 occurred near the southern end of the 1833 rupture. *Abercrombie et al.* [2003] have found that this recent event was complex: it involved rupture of the subduction interface, and a strike-slip fault within the downgoing oceanic slab. This is consistent with activity on N-S trending oceanic fractures farther to the west [*Deplus et al.*, 1998].

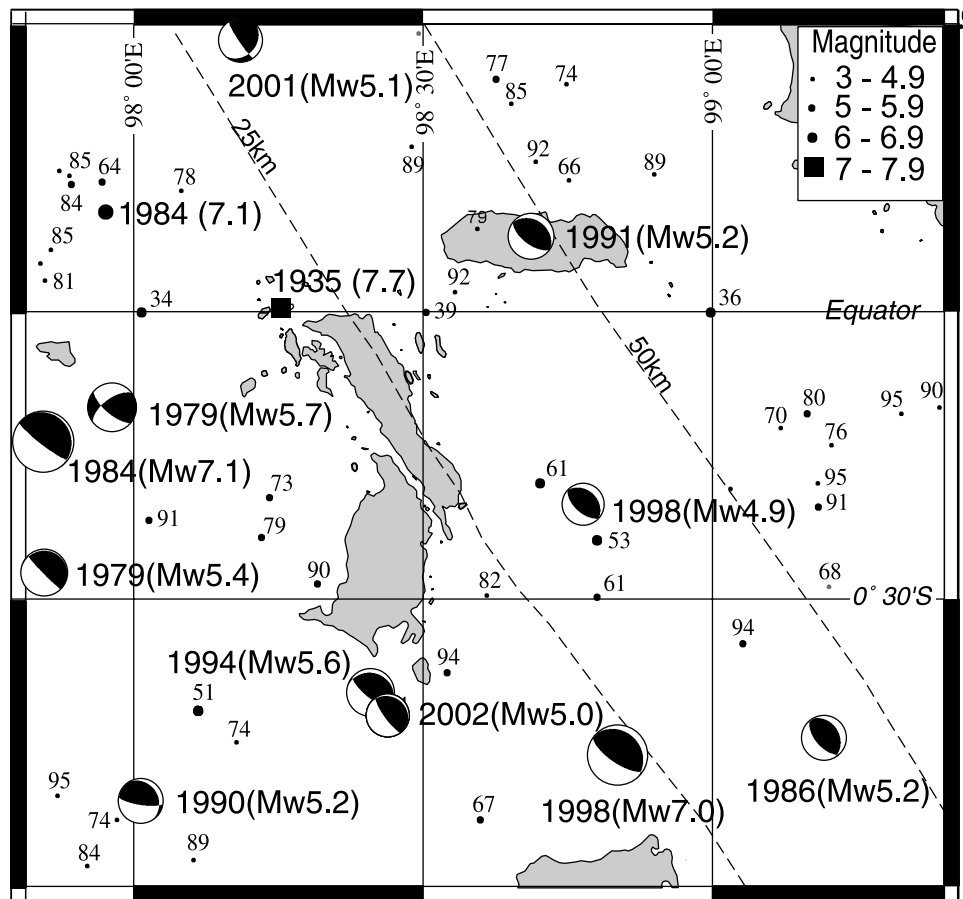[14] Recent deformation of western Sumatra has been documented by campaign-style GPS measurements made

Figure 2. Seismicity of the central Sumatran subduction zone during the twentieth century. Dots and squares are earthquake epicenters. Numbers next to dots/squares indicate year of occurrence in the twentieth century. Epicenter data from 1900 to 1963 are from NEIC. Epicenters from 1964 to 1998 are from *Engdahl et al.*'s [1998] relocations. The beach balls are Harvard double-couple solutions for earthquakes between 1976 and 2002.

between 1989 and 1994 [*Prawirodirdjo*, 2000; *Prawirodirdjo et al.*, 2000]. Their results show that the large islands south of the equator, in the area of the 1833 source rupture, moved in the direction of the relative plate-motion vector. These motions indicate that the subduction interface beneath is currently fully locked [*Prawirodirdjo et al.*, 1997]. By contrast, the GPS stations on the islands around the equator, above the 1935 source, experienced motions nearly parallel to the trench. These surface movements indicate significant aseismic slip on the interface. This part of the subduction interface is within *Sieh and Natawidjaja*'s [2000] central tectonic domain, where the overriding plate is structurally more complex than it is further south.

2. Results

2.1. Paleogeodetic Sites

[15] In 1997, 1999, and 2000, we surveyed and collected 27 coral slabs from 16 sites, near the equator (Figure 3). Most of the slabs provide time series of sea level for the past half-century. Eight of the bigger slabs enable reconstruction of sea level history for almost the entire twentieth century. Together, these paleogeodetic data reveal the pattern of vertical deformation for the 1935 event, as well

as the pattern of continuous slow deformation before and after.

[16] It would be too onerous a task for you, the reader, to plow through the descriptions of all 16 sites and all 27 slabs with respect to their tectonic significance. Therefore we present below detailed descriptions of only three of the sites and their slabs. Detailed descriptions of the other 13 sites and their paleogeodetic records, however, are presented by *Natawidjaja* [2003] (the electronic thesis dissertation is available at http://etd.caltech.edu/etd/available/etd-05222003-155554/). After presenting the three sites, we present their HLS time series along with the time series from the other 13 sites. We then discuss the uncertainties in the records and correct them for global changes in sea level before interpreting the HLS histories with respect to tectonic.

2.1.1. Bendera Site (Tb)

[17] Our westernmost site, nearest the trench, is in Bendera Bay, near the western tip of Tanabala Island (Figure 3). The bay is 2.5 km wide and opens only to the north. Figure 4a is a map of the eastern shore of the bay. In general, the intertidal reef flat is about 100 m wide. Loose cobbles and small boulders that litter the outer part of the intertidal reef may well have been emplaced by a tsunami. Mangrove forest occupies most of the intertidal region.
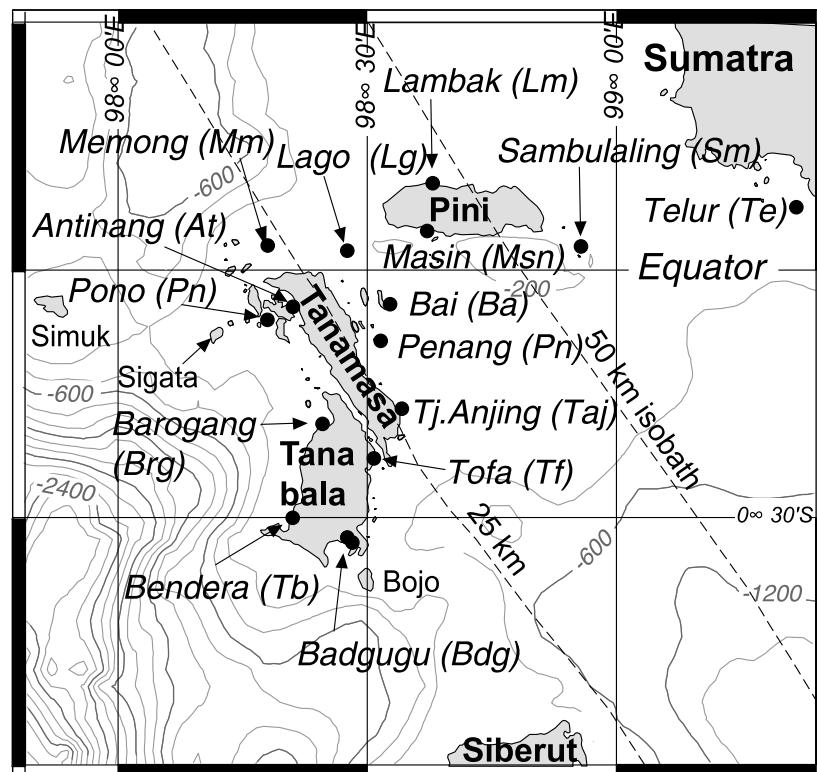
Figure 3. Index map of paleogeodetic sites. Bathymetry is from GTOPO 30. Isobaths of Wadati-Benioff zone are adapted from *Sieh and Natawidjaja* [2000].

Populations of both modern, living *Porites* microatolls and fossil *Porites* heads are present. Slabs from specimens representing each of these two populations enable construction of the site's HLS history for the entire twentieth century.

[18] The richest zone of dead, well-preserved heads sits on a promontory at the mouth of a small embayment (Figure 4a). This graveyard of dead cup-shaped *Porites* microatolls stands above the sea during low low tide (Figure 4b). Numerous large, living *Porites* microatolls grow on a more protected spot, further east within this small embayment. Well-preserved crests of the dead microatolls have nearly concordant elevations, about 55 cm above the elevations of the crests of the living microatolls (Figure 4c). Thus it appears that an uplift of at least 55 cm has occurred. Head H18, which rests on the pebbly substrate between the principal fields of dead and living heads, exhibits both a raised, dead inner core and a living, lower partial rim (Figure 4c). Thus it suggests that the upper half-meter or so of this colony was raised above HLS, but the lower portions of the head remained below HLS. This lower perimeter of the head was thus able to survive and grow for many years after the uplift event, as described for microatolls elsewhere with a similar morphology by *Taylor et al.* [1987] and *Zachariasen et al.* [2000].

2.1.1.1. Fossil Heads

[19] The family of dead microatolls resting on the promontory range in diameter from 150 to 250 cm and rise 20 to 40 cm above the substrate. We cut a slab sample from one of these heads, H1 (Figure 4c). Unlike most of our slabs, this one spans the entire diameter of the microatoll (Figure 5a). Therefore it affords the unusual opportunity of comparing the HLS histories derived from two radii of the same head.

[20] The annual bands in this head are exceptionally clear (Figure 5b), so there are no ambiguities in the relative ages of bands. Figure 5c shows that the recovered bands grew over a period of 50 years. In the cross section, the head appears to have begun as two separate, asymmetric heads. However, the microatoll is quite circular in plan view, so it may be that the two halves of the head seen in the cross section grew from an older raised rim, below the recovered part of the head.

[21] U-Th analysis of a sample from the 29th band in from the perimeter of the microatoll yielded a date AD 1897 ± 8 (Table 1). Thus, the outermost band formed AD 1926 ± 8. This date is essentially consistent with a date of death of 1935, the date of the largest earthquake in this region in the past 140 years [*Rivera et al.*, 2002]. We assumed this date for the outermost ring in assigning the band dates that appear on the cross section.

[22] The cross section shows clearly a general submergence trend throughout the last 35 years of microatoll growth (Figure 5c). The head grew freely upward and outward from before the turn of the century until 1900. The first HLS impingement on the top of the head occurred in 1901. Upward growth then appears to have resumed until another impingement occurred at a higher level in about 1905 and then resumed again until a later impingement between 1914 and 1925. Upward growth then resumed until an impingement at a still higher level in about 1931. Complete emergence killed the microatoll in 1935.

[23] Figure 5d displays the HLS data graphically and allows us to compare and contrast the history revealed by each side of the head and the overgrowth in the middle of the head. The large dots indicate HLS levels, where the tops
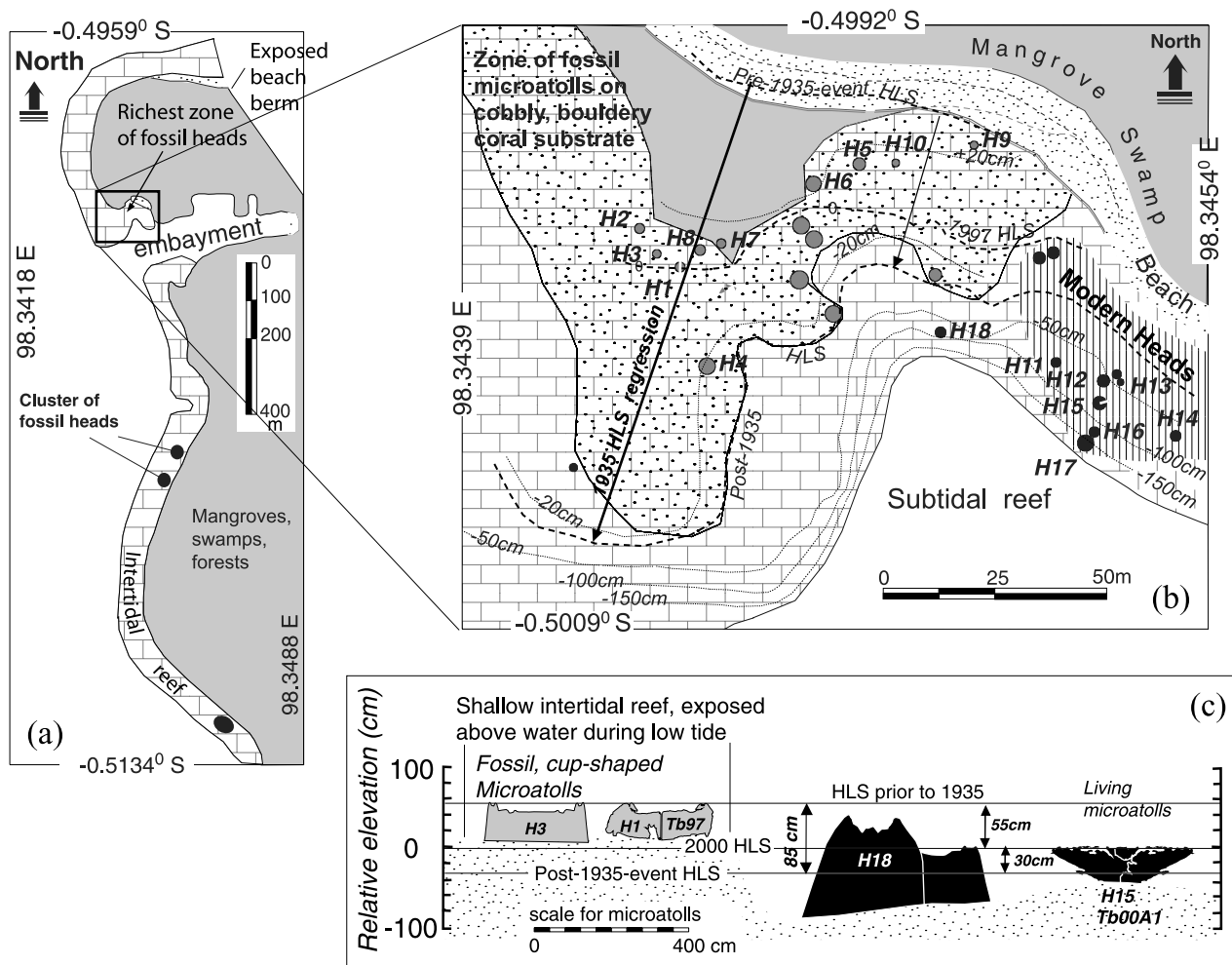
Figure 4. (a) Setting of the Bendera site, on the eastern shore of Bendera bay, southwest Tanabala Island. (b) Detailed site map. Sudden emergence during the 1935 event raised the entirety of the intertidal reef above the lowest tide level and killed the ancient microatolls. White bars on H1 and H15 indicate the locations of coral slabs collected in mid-1997 and mid-2000 field surveys. (c) Three types of microatolls at the Bendera site. Fossil microatolls rose entirely above the intertidal zone during the 1935 event and died. H15 and H18 were only partially exposed, so their lower parts survived the event.

of the coral bands were killed by the annual lowest tides. The bars, small squares and diamonds represent HLS surfaces that have undergone a little bioerosion. The smaller triangles and dots are elevations of the tops of coral bands that grew freely outward and upward, below the HLS.

[24] Although all the histories are similar, discrepancies of as much as 5 cm are apparent. For example, the HLSs recorded on the right side of the head are up to 3 cm higher than those recorded on the left. This is either an indication of a true difference in the HLS across the top of the head or

bioerosion on the left side of the coral surface. On the basis of the shape of the surface across the head, we favor the latter interpretation. Intensive bioerosion commonly occurs on the dead central part of a microatoll and obscures the original shape of the old coral surfaces [e.g., *Scoffin and Stoddart*, 1978; *Woodroffe and McLean*, 1990; *Zachariasen et al.*, 1999].

[25] Although the apparent HLS elevations vary a little from side to side, HLS impingement dates and periods of free upward growth are nearly the same throughout the head

Figure 5. (a) Sampled ancient microatoll (H1/Tb97). The cup-shaped geometry implies that rapid submergence was occurring in the decades prior to the 1935 event. (b) X-radiograph of the coral slab. The annual banding is exceptionally clear, so there are no ambiguities in the relative ages. Visual ring counting assumes the exterior band grew in 1934, which is consistent with the U-Th age (1897 ± 8). (c) Drawing of the Tb97 slab. The cross section permits the comparison of HLS histories from the two radii. (d) HLS records recovered from Tb97 as a function of time. The averaged submergence rates are determined by least squares fits of the entire or partial HLS records. The least squares fit to all the HLS records from 1900 to 1935 yields a submergence rate of 5.4 mm/yr. The least squares fit to well-preserved HLSs yields a submergence rate of only 4.5 mm/yr.

(Figure 5d). Combining the HLS impingements from all sides, we calculate an average submergence rate from 1901 to 1935 of about 5.4 mm/yr. If we calculate an average rate using only the HLS where it is clearly uneroded, then the average submergence rate from 1901 to 1935 is ~4.5 mm/yr. In fact, the submergence rate is probably not constant. It appears that the HLS was close to being stable from 1914 to 1925. In contrast, before and after this period, submergence
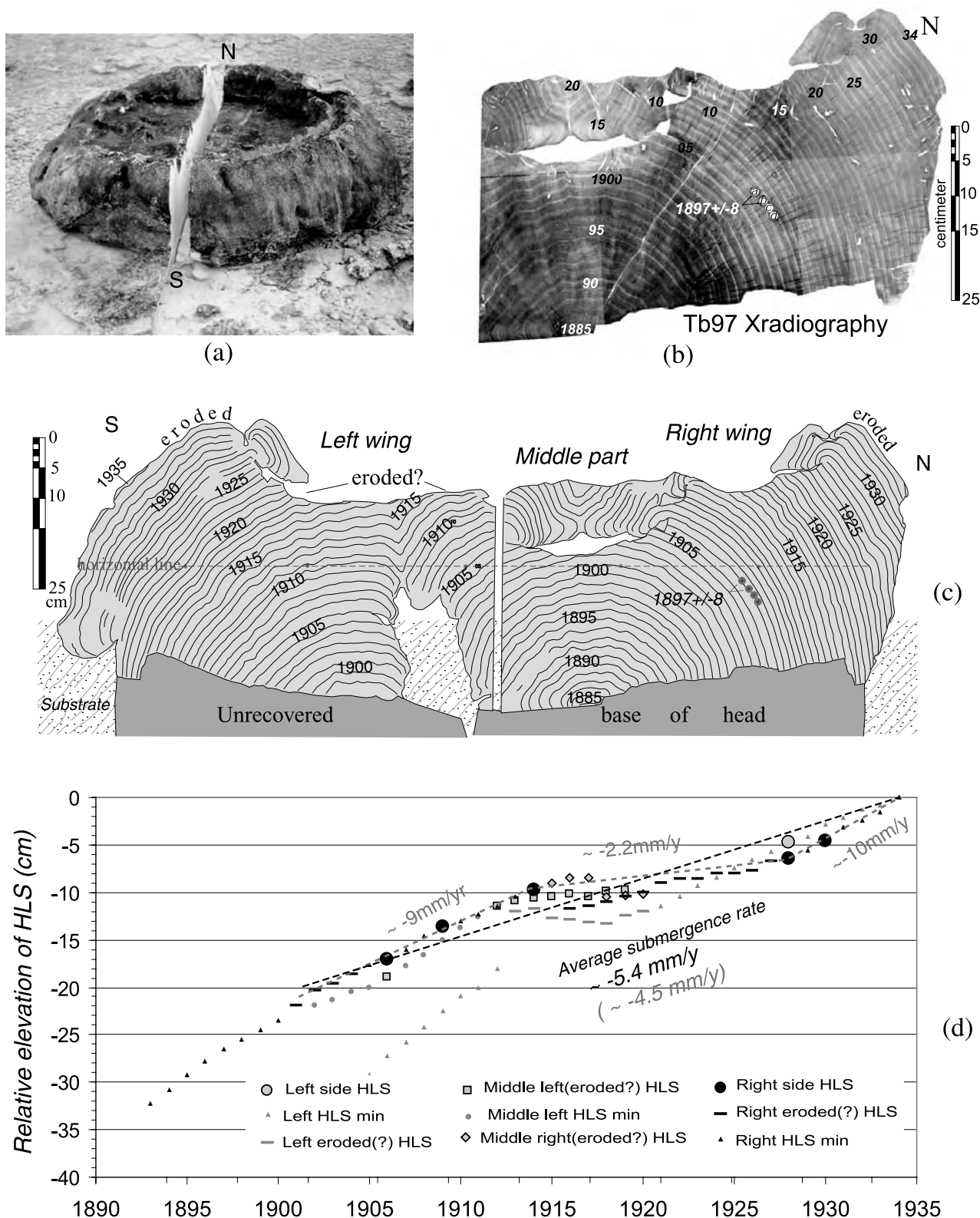

Figure 5.

Table 1. The ^{230}Th Ages of Central Sumatran Microatolls[a]

Site	Sample	^{238}U, ppb	^{232}Th, ppt	δ^{234}U Measured	^{230}Th/^{238}U Activity Ratio	^{230}Th Age Uncorrected	^{230}Th Age Corrected	Calendar Year	δ^{234}U$_{initial}$ Corrected
Bendera	Tb-97	2672 ± 3	778 ± 4	151 ± 1.1	0.00118 ± 0.000011	111.4 ± 1.0	104.1 ± 8	1894/-	151.8 ± 1.1
	Tb00A1-3a	2418 ± 3	1176 ± 11	145.9 ± 1.1	0.00074 ± 0.00002	70 ± 2	52 ± 20	1949/1931	145.9 ± 1.1
E.Badgugu	Bdg00B1-2b	2205 ± 2	340 ± 17	145.9 ± 1.1	0.00046 ± 0.00003	44 ± 2	38 ± 8	1963/1963	145.9 ± 1.1
	Bdg00B1-3b	2232 ± 9	183 ± 17	145.4 ± 4.1	0.00128 ± 0.00003	122 ± 3	119 ± 6	1882/1927	145.4 ± 4.1
	Bdg00B1-3a	2093 ± 4	595 ± 9	147.0 ± 2.1	0.00090 ± 0.00003	85 ± 3	75 ± 11	1926/1927	147.0 ± 2.1
	Bdg00B-1-4b	2352 ± 4	685 ± 7	144.8 ± 1.7	0.00105 ± 0.00003	100 ± 2	89 ± 11	1912/1915	144.9 ± 1.7
Barogang	Brg00A1-2a	2471 ± 3	184 ± 9	147.3 ± 1.5	0.00053 ± 0.00002	50 ± 1	48 ± 4	1953/1953	147.4 ± 1.5
	Brg00A1-3a	2330 ± 2	125 ± 10	147.1 ± 0.9	0.00087 ± 0.00002	82 ± 2	80 ± 4	1921/1916	147.2 ± 0.9
Pono	Pn00A3-4b	2362 ± 2	283 ± 9	147.0 ± 0.8	0.00080 ± 0.00002	76 ± 2	72 ± 6	1929/1927	147.0 ± 0.8
	Pn00A3-5b	2319 ± 2	108 ± 11	146.1 ± 1.1	0.00048 ± 0.00002	46 ± 2	44 ± 4	1957/1958	146.1 ± 1.1
	Pn00A3-2b	2216 ± 6	108 ± 10	147.6 ± 2.9	0.00072 ± 0.00003	69 ± 3	67 ± 4	1934/1936	147.7 ± 2.9
	Pn00A3-2b	2390 ± 3	85 ± 7	146.3 ± 1.5	0.00072 ± 0.00002	69 ± 2	68 ± 2	1933/1936	146.3 ± 1.5
Antinang	At99A1-2	2680 ± 3	588 ± 20	146.1 ± 1.1	0.00059 ± 0.00002	56 ± 2	51 ± 3	1948/1946	146.1 ± 1.1
Memong	Mm99A1-2	2725 ± 3	458 ± 13	146.2 ± 1.0	0.00086 ± 0.00003	82 ± 3	78 ± 4	1922/-	146.2 ± 1.1
	Mm99A1-4	2572 ± 3	365 ± 10	147.9 ± 1.1	0.00147 ± 0.00002	140 ± 2	136 ± 3	1864/-	147.9 ± 1.1
	Mm00A1-2b	2425 ± 2	70 ± 11	147.2 ± 1.1	0.00073 ± 0.00002	70 ± 2	69 ± 3	1932/1933	147.2 ± 1.1
	Mm00A1-3b	2582 ± 3	194 ± 12	146.0 ± 1.8	0.00151 ± 0.00003	144 ± 3	141 ± 6	1860/1865	146.1 ± 1.8
Tofa	Tf99C1-2	2584± 2	4251 ± 37	144.6 ± 1.1	0.00109 ± 0.0002	104 ± 2	62 ± 21	1938/1947	144.7 ± 1.1
Tj. Anjing	Taj00A1-2a	2238 ± 3	1177 ± 11	145.0 ± 2.0	0.00086 ± 0.00004	82 ± 4	62 ± 23	1939/1959	145.0 ± 2.0
	Taj00A1-4b	2248 ± 4	151 ± 9	145.0 ± 2.3	0.00085 ± 0.0003	81 ± 2	78 ± 5	1923/1939	145.1 ± 2.3
	Taj00A1-3b	2350 ± 4	230 ± 9	145.6 ± 2.2	0.00072 ± 0.00002	69 ± 2	65 ± 4	1936/1941	145.7 ± 2.
	Taj00A1-4a	2226 ± 3	121 ± 5	145.1 ± 1.6	0.00078 ± 0.000002	75 ± 2	73 ± 3	1928/1939	145.1 ± 1.6
	Taj00A1-5b	2335 ± 2	198 ± 9	146.5 ± 1.0	0.00107 ± 0.00002	102 ± 2	99 ± 5	1902/1912	146.5 ± 1.0
Lago	Lg99A1-3	2723 ± 3	135 ± 9	146.6 ± 1.1	0.00064 ± 0.00003	61 ± 3	60 ± 3	1940/1943	146.6 ± 1.1
	Lg99A1-2a								
	Lg00A1-1b	2714 ± 3	166 ± 10	147.3 ± 1.3	0.00071 ± 0.00002	67 ± 2	65 ± 4	1936/1936	147.3 ± 1.3
	Lg00A1-2a	2567 ± 2	122 ± 11	146.3 ± 1.1	0.00129 ± 0.00002	123 ± 2	121 ± 4	1880/1882	146.4 ± 1.1
Lambak	Lm99A1-1a	2620 ± 6	227 ± 9	144.4 ± 3.0	0.00016 ± 0.00002	15 ± 1	13 ± 2	1987/1986	144.4 ± 3.0
Sambulaling	Sm97-2-2d	2565. ± 4.0	233 ± 2.4	151 ± 1.1	0.000993 ± .000008	93.8 ± 0.8	91 ± 1.4	1907/-	151.2 ± 1.2
	Sm97-2-1b	2611 ± 3.8	117.1 ± 2.5	151.7 ± 1.2	0.00064 ± .000006	60.9 ± 0.8	60 ± 0.8	1938/-	151.2 ± 1.2

[a]Small samples from interiors of microatolls have been dated by the U-Th disequilibrium method (modifications of the *Edwards et al.* [1987] method as described by *Cheng et al.* [2000]), performed at the University of Minnesota. In the "^{232}Th" column, "ppt" refers to parts per trillion by mass. Ages and δ^{234}U values are calculated using decay constants from *Cheng et al.* [2000]. "Uncorrected" ^{230}Th ages are calculated assuming no initial ^{230}Th. "Corrected" ^{230}Th ages are our best estimate of the true age on the basis of the samples' isotopic composition. The ages are corrected for initial ^{230}Th assuming an initial atomic ^{230}Th/^{232}Th ratio of $(6.5 \pm 6.5) \times 10^{-6}$. This value is specific to corals from this area [*Zachariasen et al.*, 1999]. Under "Calendar Year," the years on the left side of the column are determined by subtracting the corrected ^{230}Th age from the time of analysis; the years on the right side of the column (in italics) are years determined by counting annual bands visible in x-radiographs. The initial δ^{234}U value is calculated from the measured δ^{234}U value using the corrected ^{230}Th age. Sample names in italics indicate replicate analyses.

occurred at a much higher rate (~9 and ~10 mm/y respectively).

2.1.1.2. Modern Heads

[26] Living microatolls in the field east of the promontory range in diameter from 130 to 350 cm at their crests and commonly rise about a meter above the substrate. In mid-2000, the living perimeter of these heads showed that these microatolls survived the devastating regional die-off in 1997. Even though the heads survived the disaster of 1997, the living corallites died down to positions several centimeters below what would have been the natural HLS for 1997 had the environmental disaster not occurred. The survival of this family of microatolls is a remarkable exception in the region. At all other sites we visited, all or nearly all microatolls died during the event of late 1997 to early 1998.

[27] The wholesale death of the coral reefs of western Sumatra in late 1997 and early 1998 presented a complication to placing our HLS time series absolutely in time. During our 1997 field season, there was an abundance of modern coral heads alive and healthy in this region. Beautiful belts of bright purple to brown living corallites girdled the sides of microatolls. Thus the age of any growth band inside a head could be determined simply by counting

annual bands inward from the living 1997 band. When we revisited the sites and others nearby in mid-1999, most of the heads had died. This massive coral mortality occurred during the severe El-Nino Southern Oscillation (ENSO) and Indian Ocean Dipole (IOD) events of 1997–1998 as well as the severe pall of smoke that extended west over the sites from the Kalimantan and east Sumatra fires of late 1997 [e.g., *Saji et al.*, 1999]. No study has been done to ascertain exactly why the corals died. According to our interviews with local people and a preliminary investigation by local marine biologists [*Indrawadi and Efendi*, 2000], however, the coral reefs appear to have died during exceptionally severe red tides, the manifestations of sudden and rampant blooms of phytoplankton.

[28] Head H15 (Tb00A1), depicted in cross section in Figure 4c is a good example of the morphology of the living heads. Its shape is typical for cup-shaped microatolls, with the lower inner flat filled partially with thin, complex younger overgrowths. Figure 6a shows this cross section in more detail. This tracing of the slab collected from head H15 shows annual bands that formed from about 1927 to 2000. The errors shown for various annual bands indicate our estimate of potential error in counting back from the outer perimeter. The radiometric U-Th age of AD 1949 ± 20
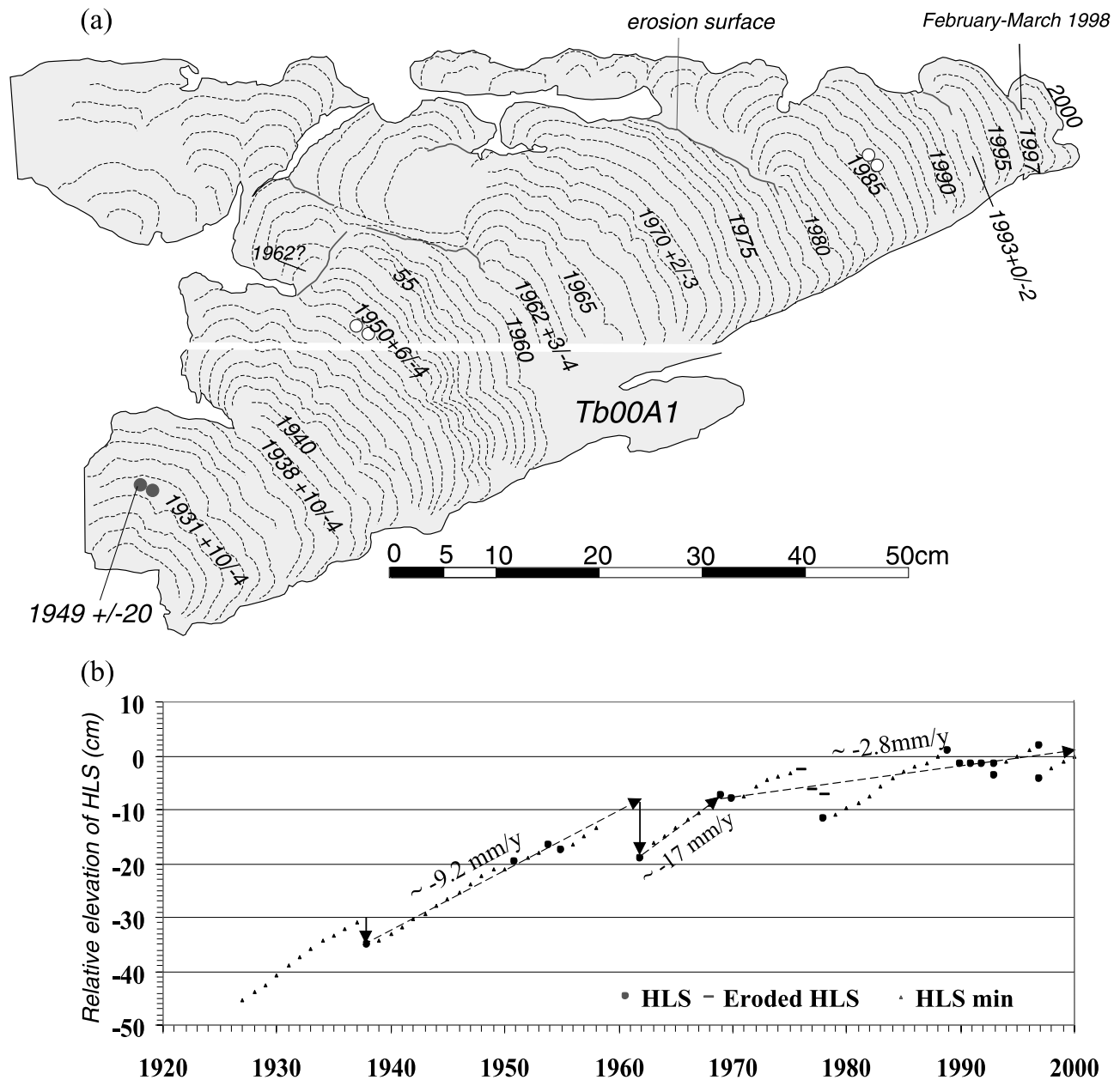
Figure 6. (a) Drawing of the x-radiograph of the Tb00A1 slab. Overall stratigraphy indicates fast submergence since about the mid-1930s. HLS impingements occurred in 1955, 1962, the mid-late 1970s, late 1980s, early 1990s, and in 1997 or early 1998. (b) HLS time series. The averaged submergence rates are from least squares fits of the parts of the HLS records indicated.

(Table 1) is consistent with our counting of the annual bands, but its large error renders the date of little value as a check on our counting.

[29] Significant deaths of the upper part of the head appear in about 1936, the early through late 1950s and early 1960s, about 1969, the mid-70s through 1980 and then several times in the 1990s, including early 1998. These impingements of HLS on the top of the head are depicted as a function of time in Figure 6b. The abundance of freely upward growing bands indicates that the head has been submerging throughout most of the past seven decades. A least squared fit to HLS impingements yields rates of about 9 mm/yr during the 1930s, 40s and 50s and about 3 mm/yr

of submergence during the 1970s, 80s and 90s. Major emergences disrupted the general submergence in the mid-1930s, the early 1960s and about 1980.

2.1.1.3. Combining the Records

[30] Figure 7 shows the HLS history of this site throughout the period spanned by both the fossil and the modern heads. The key observation is that there is an 85 cm difference in the elevation of the 1935 HLS levels between the two sampled heads. This is a measure of the emergence during the 1935 event. We use the term "event" as distinct from "earthquake," because the coral record must reflect a longer period of time than the duration of the earthquake [*Taylor et al.*, 1987]. It is more appropriate to consider this
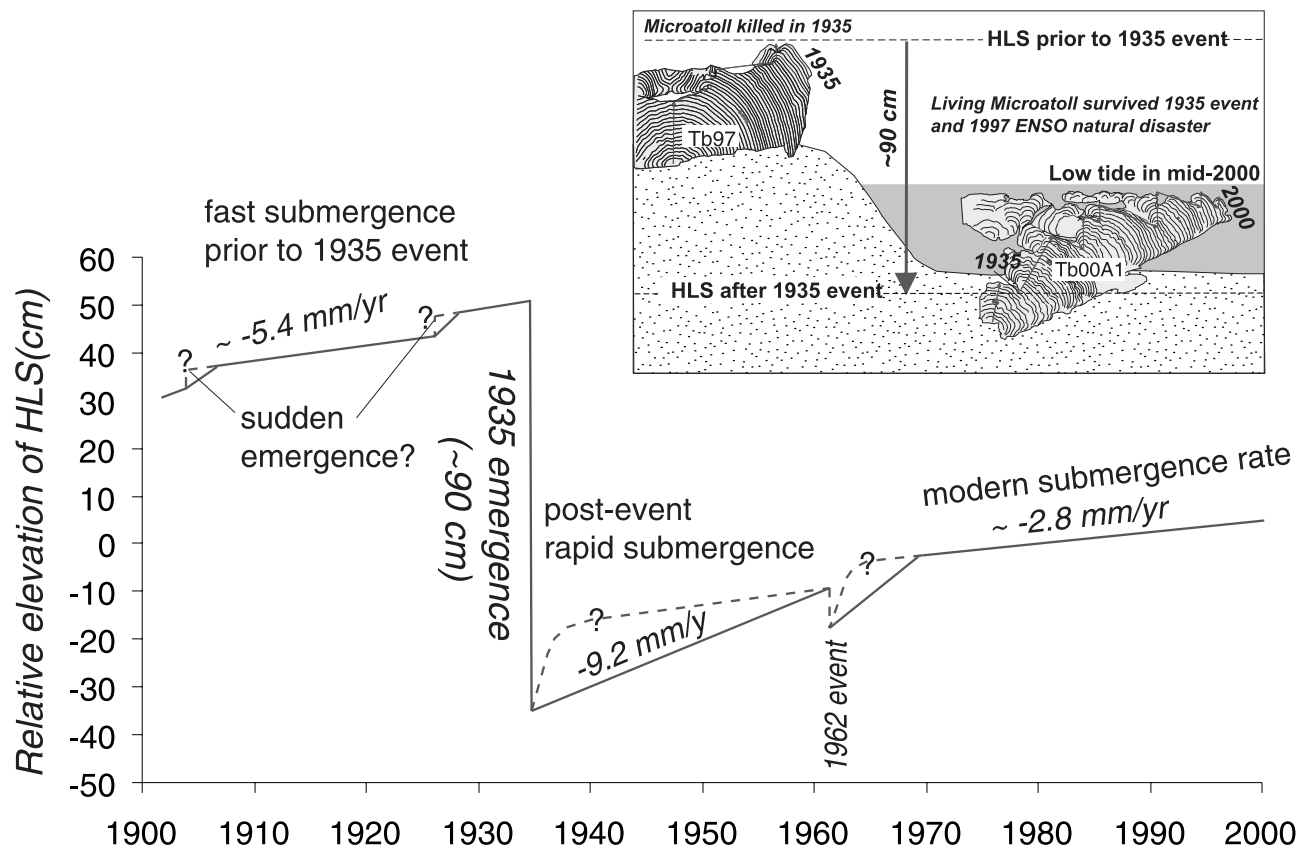
Figure 7. Combined coral stratigraphy from Tb97 and Tb00A1 slabs (inset). A principal feature is the record of the full emergence in 1935 that is measured from the crest of the ancient head's exterior to the first HLS clip in the modern microatoll. The combined HLS history recovered from the ancient and the living heads spans the entire twentieth century. A period of submergence prior to 1935 appears to have accumulated as discrete events, rather than uniformly. The fastest submergence rate occurred in the decades after the 1935 event. The 1962 event is the second largest feature and initiates a decline in the submergence rate.

value to be the net uplift that occurred during coseismic uplift and in the few months thereafter.

[31] Knowing from these heads the elevation of HLS prior to and just after the 1935 event; we can see that much of the promontory rose above HLS. Figure 4b shows that the pre-event HLS contour falls on the substrate near the foot of the modern sandy beach. The post-event HLS contour falls on the substrate 40 to 100 m seaward of the modern beach. Thus it appears that almost the entirety of the reef flat rose above HLS in 1935.

[32] In addition to the magnitude of emergence during the 1935 event, the two HLS records reveal that the pre-seismic average rate of submergence (∼5.4 mm/yr) is nearly twice the current average rate (∼2.8 mm/yr). Furthermore, it appears that the average rate of submergence in the 25 years after the 1935 event was higher still (∼9.2 mm/yr).

[33] This time series will be of use in understanding the accumulation and relief of strain in the Sumatran subduction zone. However, it represents vertical deformation at only one point above the subduction interface. In the sections that follow, we describe two other sites where we have recovered records of the 1935 event and the decades before and after. Then we present the time series recovered from these three and the 13 remaining sites. Once we have described the time series from all 16 sites, we will be in a better position to model the source parameters of the 1935 event and the processes responsible for the pre-seismic and post-seismic signals as well.
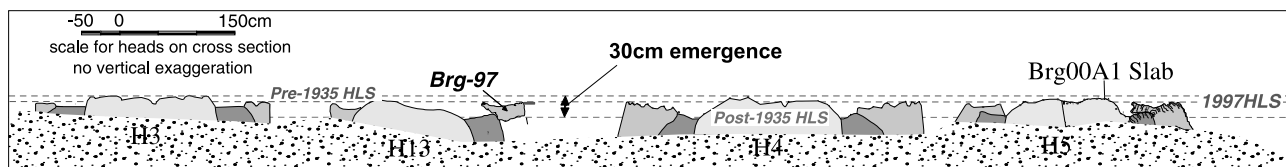
2.1.2. Barogang Site (Brg)
2.1.2.1. Coral Morphology

[34] The Barogang site, about 113 km from the trench axis, occupies the shallow reef flat on the island's northeast shore (Figure 8a). This site has many "hat shaped" heads that were living until the late 1990s and that record a large emergence in 1935 (Figure 8b). The brims of these hat-shaped microatolls consist of upward growth that has occurred in the years since 1935. The main body of these hats consists of growth that occurred prior to 1935. This morphology results from partial emergence of the micro-atolls in 1935. Thus these heads contain an HLS history that encompasses the 1935 event and the decades before and after. The bowl of each hat represents coral growth before emergence in 1935 and the brims record subsequent growth upward and outward in decades after 1935. The vertical distance from the top of the bowl to the base of the brim is about 30 cm (Figure 8b). Thus, at first glance the magnitude of the 1935 emergence appears to be about 30 cm.

[35] The family of modern hat-shaped *Porites* heads resides on a steeper and deeper section of the shallow intertidal reef and is well protected behind a 10- to 20-m-
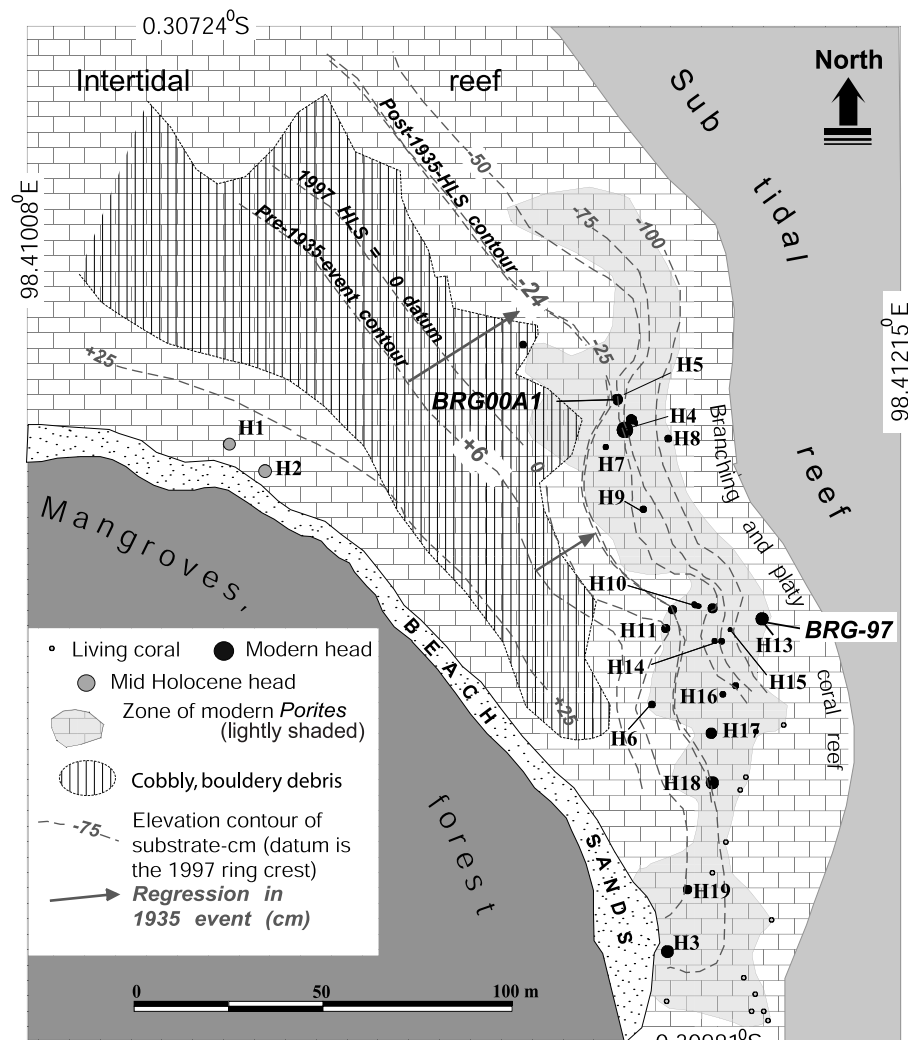
(a)

(b)

Figure 8. (a) Barogang site map. During the 1935 event the intertidal reef rose about 30 cm, thus lowering HLS from +6 cm above to −24 cm below the 1997 ring crest. Numerous modern heads display a hat-shaped morphology, which testifies to the 1935 emergence. (b) Cross sections of the hat-shaped microatolls. The heads consist of three principal parts: a central bowl, a lower brim, and an upper brim. Difference in heights of the bowl and the lower brim indicates the magnitude of emergence.

wide zone of predominantly branching, foliose and platy corals along the outer edge of the reef (Figure 8a). The heads have diameters ranging from 3 to 4 m and rise about 30 to 60 cm above the substrate. These heads were still alive and healthy when we first visited the site in 1997, but none of them showed living perimeters when we visited again in July 2000. Thus they died in the period between August 1997 and July 2000. We assume that their

final death occurred during the reef disaster of 1997–1998.

[36] Summits of the central bowls of the hat-shaped heads are remarkably concordant, with differences of less than ±4 cm (2σ). Summits of the brims are also concordant within ±4 cm (2σ) but at an elevation about 5 cm lower than the tops of the bowls. In a crude sense, this implies that the upward growth of the brims in the past several decades has
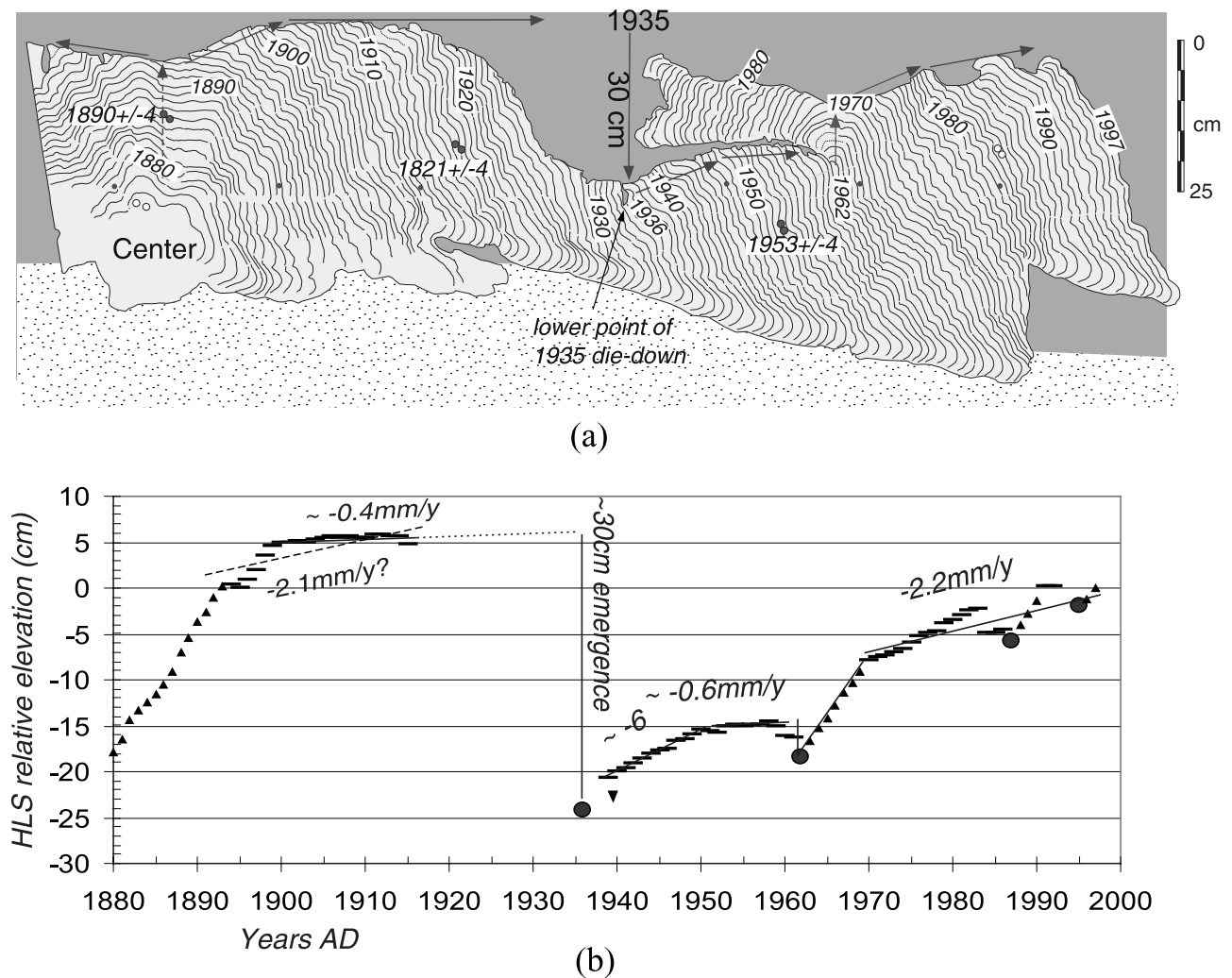
(a)

(b)

Figure 9. (a) Drawing of the BrG00A1 X-radiograph, showing the banding of the hat-shaped head. An emergence of about 30 cm during the 1935 event killed the upper half of the central bowl. The brim's topography indicates general fast submergence from 1935 until recently. Significant erosion of the bowl removed much of the upper part of the 1920 to 1935 bands. (b) HLS history reconstructed from the slab. A relatively stable period persisted for a few decades prior to 1935. Rapid submergence followed the 1935 event. Submergence appears to have diminished gradually to a much lower rate prior to 1961. The rapid or sudden submergence in 1962 is the second largest event in the HLS time series.

almost fully recovered the effect of the large emergence in 1935.

[37] Many of the hat-shaped microatolls are broken. Most of the upper surfaces of the central bowls have been degraded and rounded, especially around the edges, by bioerosion. The most prominent exception is head H3, half buried near the beach berm and still exhibiting concentric rings atop the bowl (Figure 8b). Average elevations of the top of the H3 bowl are, in fact, a few centimeters higher than that of the rest of the hat-shaped heads. This is confirmation that erosion on most of the upper surfaces of the hat-shaped heads has diminished their elevations slightly.

[38] One of the hat-shaped heads in Figure 8b shows a tilted bowl (H13). The 1935 emergence killed the raised (left) half of the central bowl but not the lower (right) half of the perimeter that was under the lowered HLS. The tilting must have occurred during or shortly after the 1935 emer-

gence. Subsequently the brims grew asymmetrically around the perimeter and remain untilted.

2.1.2.2. Paleogeodetic Records

[39] In July 2000, we took a slab from head H5 (Brg00A1) as a good representative of the family of the hat-shaped heads. The slab spans the HLS history for the entire twentieth century and the last decade of the nineteenth century. The positive print of the radiograph of the slab exhibits an extraordinarily sharp contrast between annual pairs of high-density (dark) and low-density (light) bands [*Natawidjaja*, 2003]. Thus excellent annual banding ensured very accurate visual ring counting. However, as a test of our ring counting, we performed U-Th-disequilibrium dating of samples taken from the AD 1952, 1918 and 1888 rings (Figure 9a). The U-Th dates 1953 ± 4 (2σ), 1921 ± 4 (2σ), and 1890 ± 4 (2σ) (Table 1), respectively, confirm the reliability of dates assigned by our visual counting of the annual bands.

[40] Inspection of the slab shows that the large emergence occurred sometime between AD 1927 and 1936 (Figure 9a). The precise date of the emergence cannot be determined by inspection of the rings, because the rings in this span of years clearly have suffered modest erosion on the perimeter wall of the inner head. We can conclude that the emergence antedates 1936, because beginning in that year, the slab shows upward growth toward a higher HLS. The 1927–1936 constraint that the slab imposes on the date of the event is consistent with the date of the largest earthquake in this region on 28 December 1935.

[41] Exact reconstruction of the amount of emergence associated with the 1935 event is also obscured by the erosion of the annual bands in the 1920s and 1930s. Because of the erosion of the pre-1935 bands, for example, we cannot rule out the possibility that emergence began in the years just prior to 1935. If we assume, nonetheless, that the entire emergence occurred during the December 1935 event, we can project the trend of nearly stable HLS for the first three decades of the twentieth century forward to 1935 and determine an HLS elevation. The elevation difference between this point and the base of the brim is about 30 cm (Figure 9). This, we suggest, represents the total emergence during the 1935 event.

[42] The upper surface of the microatoll has suffered from bioerosion, for we do not, in general, see the concentric ridges and swales that exist on uneroded heads (Figure 9a). Nonetheless, bioerosion appears modest, except from about 1915 to 1935, and the gross pattern of HLS ups and downs is clear. A steep slope atop the annual bands that formed between AD 1894 and 1902 indicates a few years of fast submergence around the turn of the century. The HLS between about 1902 and 1915 is nearly stable at an average rate of about −0.4 mm/yr (Figure 9b). We are not certain that this rate persisted through the 1920s and early 1930s, because of the large amount of bioerosion of the tops of those annual bands. However, we suspect that a low rate of submergence did persist up to 1935, because a nearby microatoll, H3, appears to record a low rate right up to the emergent event. We carefully surveyed the elevations of H3's preserved concentric ridges and troughs atop the upper surface of the bowl. A least squares fit to surveyed elevations along the 45 cm surface yields an average rate of about 0.8 mm/yr submergence [Natawidjaja, 2003]. This is our best estimate for the average submergence rate for the 33 years prior to 1935.

[43] The geometry of the surface of the brim exhibits predominantly fast submergence during the several decades following 1935 (Figure 9a). The total submergence is about 25 cm, but this did not accumulate uniformly. In the first three decades after the 1935 event, initially fast submergence of about 6 mm/yr decayed to a slower rate of about 0.6 mm/yr (Figure 9b).

[44] An emergence of about 10 cm occurred in 1962. Submergence was rapid following this emergence so that 10.5 cm of unrestricted upward growth occurred before HLS again impinged on the microatoll in 1969. It is indeterminate whether this submergence occurred in a single event after the 1962 emergence or whether it occurred over a longer fraction of the 7-year-long period.

[45] Since 1969, upward coral growth has been restricted by HLS. It appears that from about 1969 to 1997, the average rate of submergence was a mere 2.2 mm/yr (Figure 9b). Small emergences in 1987 and 1995 are associated with El-Nino events in those years.

[46] We collected a slab from the upper, outer brim of another hat-shaped microatoll, Brg97 (Figure 8b). Visual counting of clear annual banding retrieves a complete time series back to AD 1962. A detailed analysis of this slab is available from Natawidjaja [2003], but only the results appear later in this paper.

[47] The HLS histories from the two slabs, Brg00A1 and Brg97, are very similar. Details differ, but by and large the dates and the values of rises and falls in HLS are consistent. In particular, elevation differences of each uneroded HLS for the 1962, 1985 and 1995 rings of the Brg97 and Brg00A1 records are generally less than 1 cm. Both heads show a diminishing of rates from the early 1970s to 1997. This is a good example the redundancy provided by multiple measurements at a site.

[48] In summary, the submergence rate at Barogang prior to 1935 was less than 1 mm/yr. During the 1935 event, an approximately 30 cm emergence occurred and killed the upper half of head H5. This was subsequently followed by a period of fast submergence freeing the coral to grow upward. Submergence, however, is not distributed evenly through the period from 1935 to 1997. The rapid submergence of the first two decades (∼6 mm/yr) seems to decay to a slower rate prior to 1961 (∼0.6 mm/yr) (Figure 9b). About 10 cm of emergence occurred in 1962, and then fast, larger submergence resumed until 1969. From 1969 to 1997 the submergence rate is much slower.

2.1.3. Lago Site (Lg)

[49] The Lago site lies on a wide intertidal flat on the northeast side of Lago Island (Figure 10a). The island is about a half kilometer in diameter and rises only about 2 m above sea level. The landward half of the intertidal flat is a deeper, sandy expanse nearly devoid of coral heads. The perimeter of the flat consists of a high-energy rampart of coral rubble and in situ branching corals. A wide field of massive *Porites* heads resides between the outer rampart and the landward pool (Figure 10b).

[50] There are two basic forms of the modern heads. Those with a diameter between about 1 and 1.3 m have convex downward upper surfaces indicative of slow emergence in the past few decades. Heads H1, H4 and H16 are good representatives of this sub-population (Figure 10c). Larger heads, some with diameters as great as 3.5 m, have a cup-shaped morphology, with a lower central flat about 30 cm below a 60 cm wide raised outer rim. This morphology represents a longer HLS history dominated by a submergence event. Examples of this sub-population are Heads H14 and H17 (Figure 10c).

[51] We collected two contiguous slabs from the same southeast radius of one of the large heads, H17. We collected the outer rim in July 1999 and the central flat in July 2000. The relationship of these two slabs was established from surveying of the upper surfaces of each slab prior to removal (Figure 11a). Together, these slabs contain an HLS history that extends from about 1870 to 1997. The slabs reveal steady, slow emergence between 1870 and 1935 and from 1970 to 1997. These periods of stable emergence are interrupted by a large submergence event in 1935 and a lesser submergence in 1962.
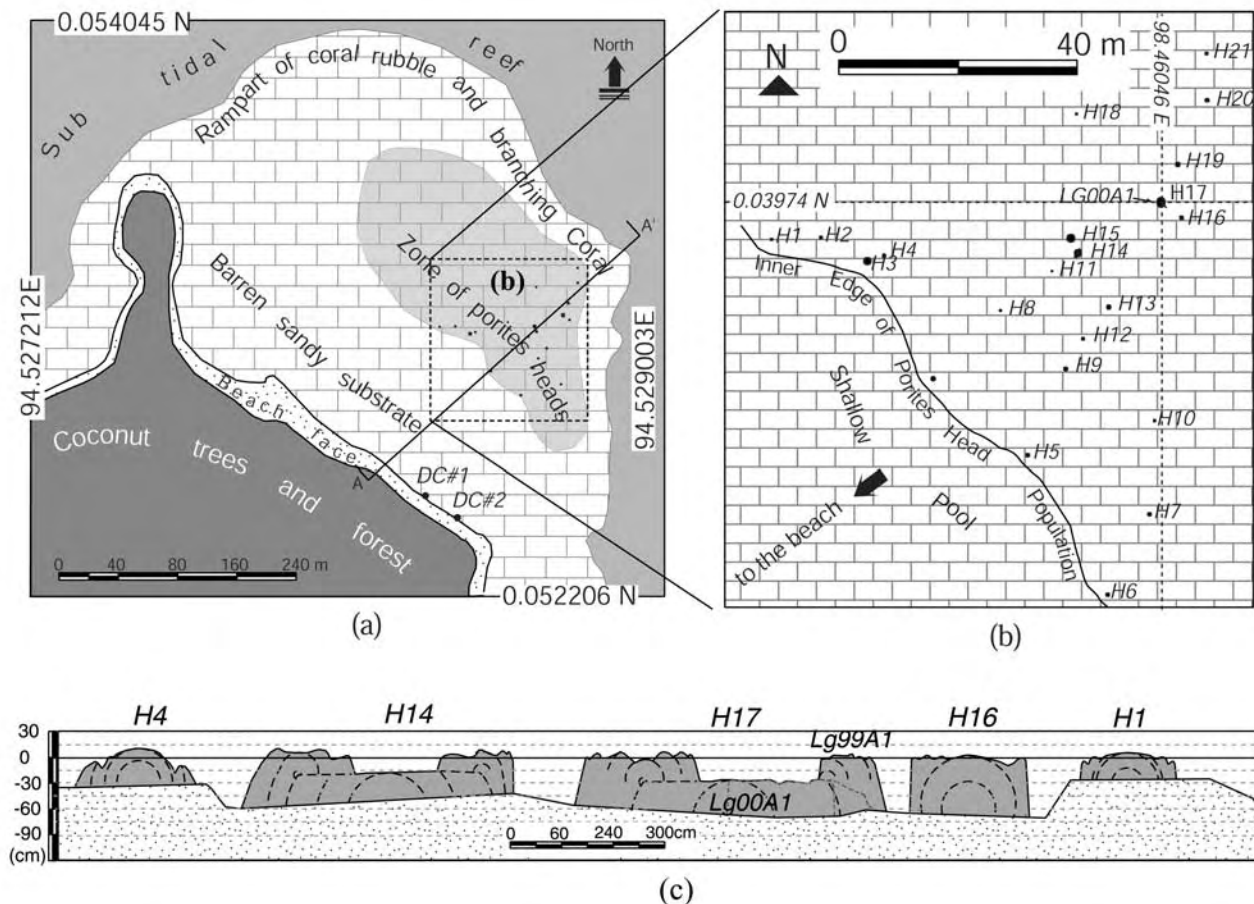
Figure 10. (a) Map of the Lago site. A field of Porites heads occurs on the broad intertidal reef flat, behind a high-energy rubbley rampart. DC#1 and DC#2 are the location of the old heads from which we took drill core samples. (b) Detailed map of the field of the modern Porites heads. (c) Profiles of five selected microatolls. Smaller heads (H1, H4, H16) formed after the large submergence event of 1935. Thus they lack a low inner flat. Their shape indicates slow emergence in the past few decades. The cup-shaped morphology of the larger heads results from about 30 cm of submergence in 1935. The low inner flats pre-date 1935, whereas the raised outer rims post-date 1935.

[52] The annual bands in H17 are exceptionally clear, so there is little ambiguity in assigning their ages by visual ring counting. We needed only to assume that the exterior ring formed in 1997. Two U-Th ages confirm the age assignments. The 1935 growth band yielded a date of 1936 ± 4, and the 1882 growth band yielded a date of 1880 ± 4 (Table 1, Figure 11a).

[53] The central flat of H17 (Lg00A1) indicates that it was slowly emerging in the decades prior to 1920 (Figure 11a). The top of the central flat is devoid of the concentric rings that are characteristic of minor annual fluctuations in HLS. This suggests that bioerosion has removed a few centimeters of the central flat. Nonetheless, the top of the central flat slopes gently away from its center. This slope yields an average rate of emergence of about 1.1 mm/yr for the period 1873 to 1935 (Figure 11b).

[54] A trough in the upper surface occurs at about the 1920 band. This exists throughout the entire 15 cm thickness of the sawed slab, so it does not appear to be an effect of bioerosion. Rather, it appears that the emergence of the

prior decades reversed in the 15 years prior to the 1935 event. The average rate of submergence in these 15 years appears to have been about 3.3 mm/yr (Figure 11b).

[55] None of the annual bands between 1935 and 1958 show HLS impingements. Instead, they display rapid, unconstrained upward growth. The difference in elevation between the 1935 and 1958 growth bands is about 28 cm (Figure 11a). We interpret this value as a rough indication of submergence magnitude during the 1935 event. However, this value also includes all post-seismic transients that might have occurred in months, years and decades after 1935. If we subtract two decades of emergence at the most recent or the pre-1935 rate, we estimate a slightly higher step associated with the 1935 event and its post-seismic transients −30 to 35 cm (Figure 11b).

[56] Just a few years after the initial post-1935 HLS impingement by the coral head, another period of free upward growth began. As at many other sites, this episode began in 1962. This upward growth ended in 1970, by which time the microatoll had grown upward an additional
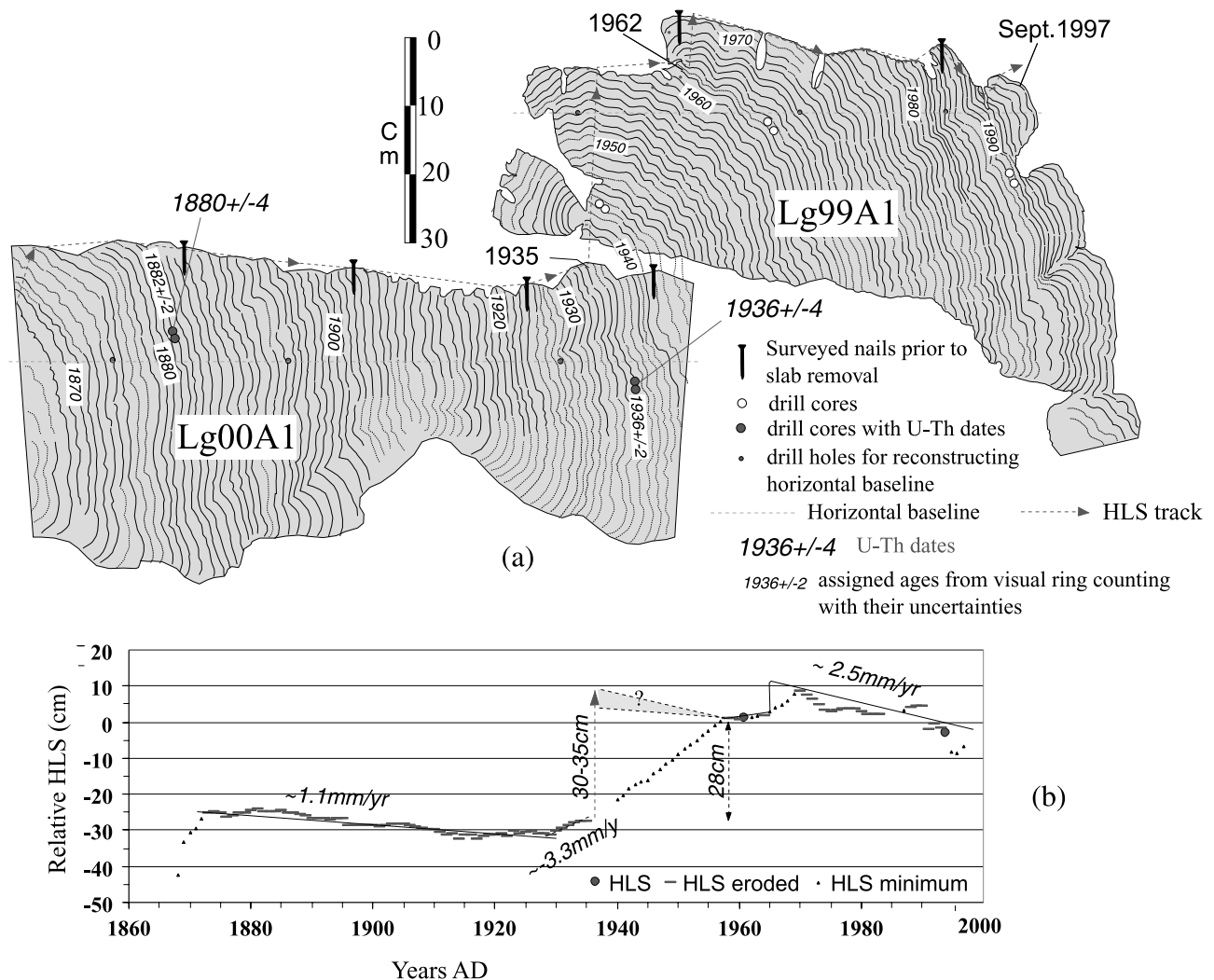
Figure 11. Slabs from head H17 (a) Two slabs, Lg99A1 and Lg00A1, collected in 1999 and 2000. The top of central lower flat suggests slow emergence site between 1873 and 1920. Sudden or rapid submergence in 1935 resulted in free upward growth of about 30 cm from 1935 to 1957. The flat top of the outer rim represent growth from about 1958 to 1961 and from 1970 to 1997. The 8 cm rise in the height outer rim between 1962 and 1970 resulted from submergence in 1962. Date assignments are based on visual ring counting, assuming the exterior band formed in 1997. (b) Plot of the HLS history recovered from Lg99A1 and Lg00A1. Note the sizes of the submergence events in 1935 and 1962 and that the post-1970 emergence rate is twice as fast the pre-1935 rate.

8 cm (Figures 11a and 11b). This is a rough measure of the magnitude of submergence during the 1962 event.

[57] For the past 30 years, the upper surface of the living perimeter of the head has been dropping at an average rate of about 2.5 mm/yr (Figure 11b). This rate is twice as fast as the average emergence rate prior to 1935.

[58] In short, the two coral slabs at Lago provide a long, continuous record of sea level change over the past 130 years. Between 1870 and 1920, the site was emerging steadily at a rate of about 1.1 mm/yr. In about 1920, this trend appears to have reversed, with submergence at an average rate of about 3.3 mm/yr continuing up to the date of the 1935 earthquake. The 1935 event and any transients in the subsequent two decades yielded a net submergence of the site of 30 to 35 cm. Submergence during the 1962 event amounted to about 8 cm. In the past three decades (1970 to

1997), emergence at an average rate of 2.5 mm/yr has been occurring.

2.2. A Synthesis of Paleogeodetic Records

2.2.1. Overview

[59] In the preceding sections, we presented examples of paleogeodetic records from coral microatolls at three sites on fringing reefs near the equator. For the sake of brevity, we do not describe the other 13 sites and their paleogeodetic records in this paper. Complete descriptions are given by *Natawidjaja* [2003]. However, we present a summary of the HLS histories of all 16 sites in Figure 12. This compilation of all the records facilitates comparison of the HLS histories by depicting them with their time scales aligned and with the same scaling of emergence and submergence relative to the modern HLS.
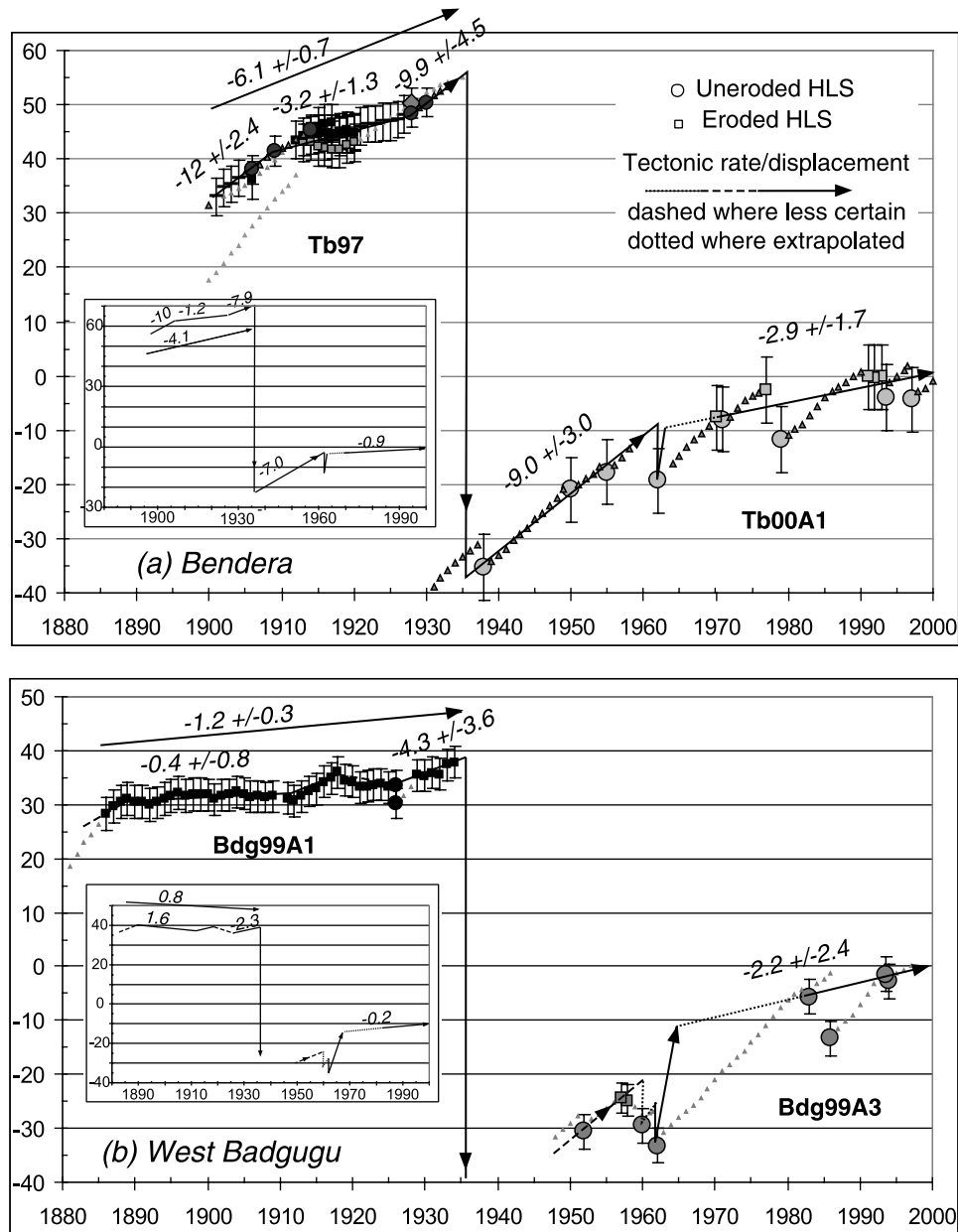
Figure 12. HLS histories of all sites, plotted with the aligned timescales and the same scaling of emergence and submergence relative to modern HLS. The 1935 event dominates the history. The 1962 event is the second largest event. The vertical deformation rates vary markedly from site to site and for different periods. Inset figures are paleogeodetic records derived from the HLS time series, but corrected for a 2 mm/yr global sea level rise.

[60] Figure 12 shows clearly that the 1935 seismic event dominates the HLS history of several of the sites. We will see that the records contain a geographically coherent pattern of submergence and emergence for this event. The 1962 aseismic event is the second largest short-lived event recorded throughout the region. It commonly appears in the records as an emergence and subsequent submergence. The emergence is mostly less than 10 cm, but the submergence has substantially larger magnitude, up to about 25 cm. The shape, magnitude and coherent regional pattern of the 1935 and 1962 events distinguish them from numerous other signals that are smaller in magnitude and in geographical extent. Figure 12 also shows that rates of aseismic vertical deformation during the century vary markedly from site to site. Moreover, many sites show abrupt changes in rate associated with the events of 1935 and 1962.

2.2.2. Uncertainties in the Coral Paleogeodetic Records

[61] In previous sections, we did not discuss in detail the sources of uncertainty inherent in our microatoll data. The analysis that we embark upon in the following sections requires, however, that we do so now. Accurate determination of the magnitude of deformation in 1935 and 1962, for example, requires determination of the uncertainties in the
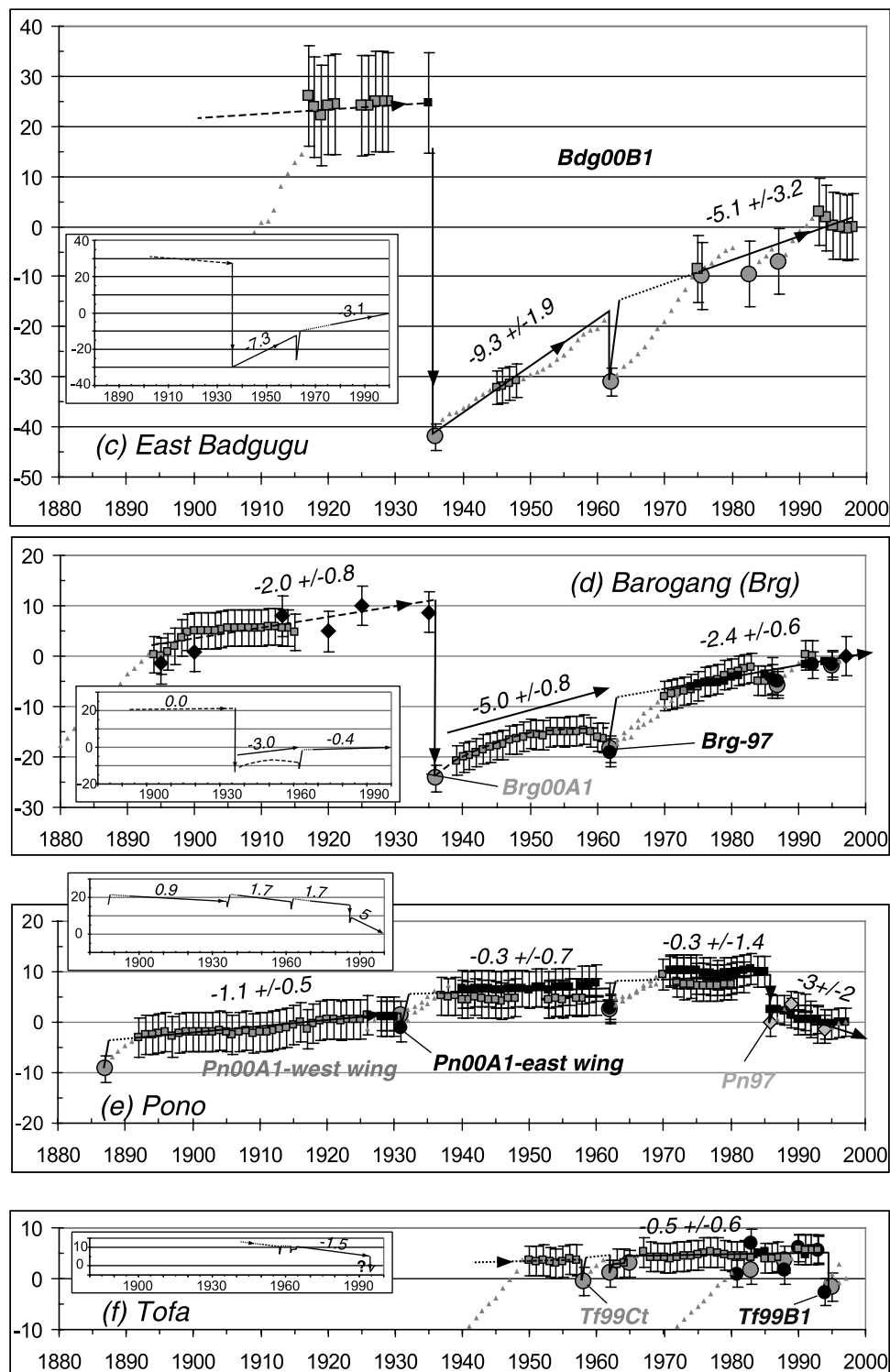
Figure 12. (continued)

levels of HLS both before and after these events. Similarly, calculations of rates of submergence and emergence during the remainder of the century require knowledge of the uncertainties in the data. These errors are incorporated in the HLS curves of Figure 12. These curves are then used to model slip on the subduction interface associated with deformation during the 1935 earthquake, the 1962 aseismic event, and the remainder of the twentieth century. In the

following paragraphs, we will discuss procedures to calculate the uncertainties that we use in Figure 12.

[62] Paleogeodetic records from microatolls contain two principal sources of uncertainty. One source is nontectonically induced variations in HLS. The other is the erosion of the upper surfaces of microatolls. Errors associated with the former are relatively easy to quantify. Errors due to erosion, however, are more difficult to assess. Once both eroded and uneroded data
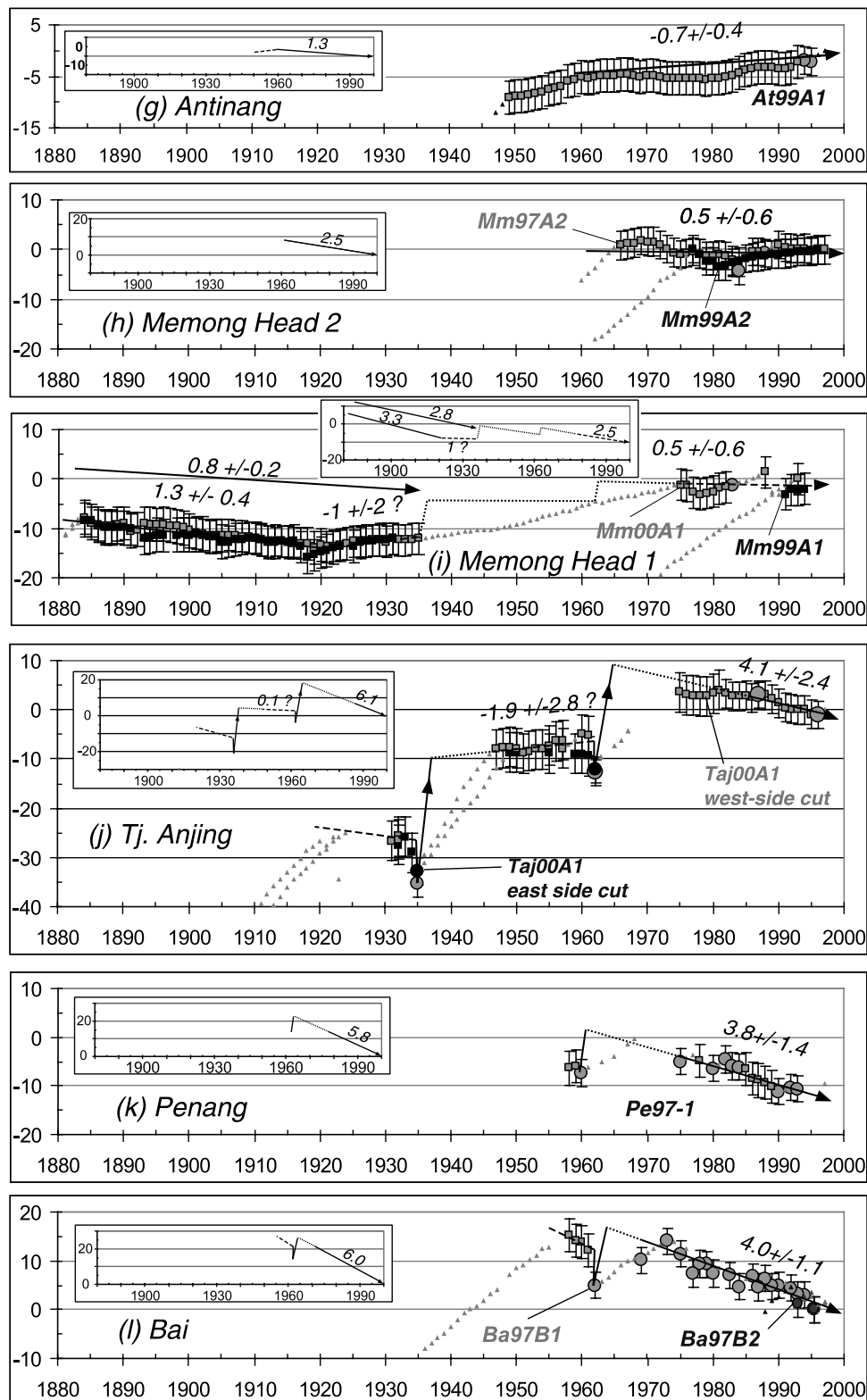
Figure 12. (continued)

points have been assigned errors, rates of submergence and emergence can be determined by use of linear regressions.

2.2.2.1. Uncertainties Associated With Nontectonic Fluctuations

[63] A microatoll's HLS record is not, ipso facto, a record of tectonism, but serves as a proxy record of lowest annual low tides [*Taylor et al.*, 1987; *Zachariasen et al.*, 1999, 2000]. Hence tectonic phenomena as well as nontectonic sources, such as global hydroisostatic changes in sea level, regional oceanographic oscillations, and local variations in upward growth rate all contribute to HLS history. Thus these nontectonic signals in HLS history
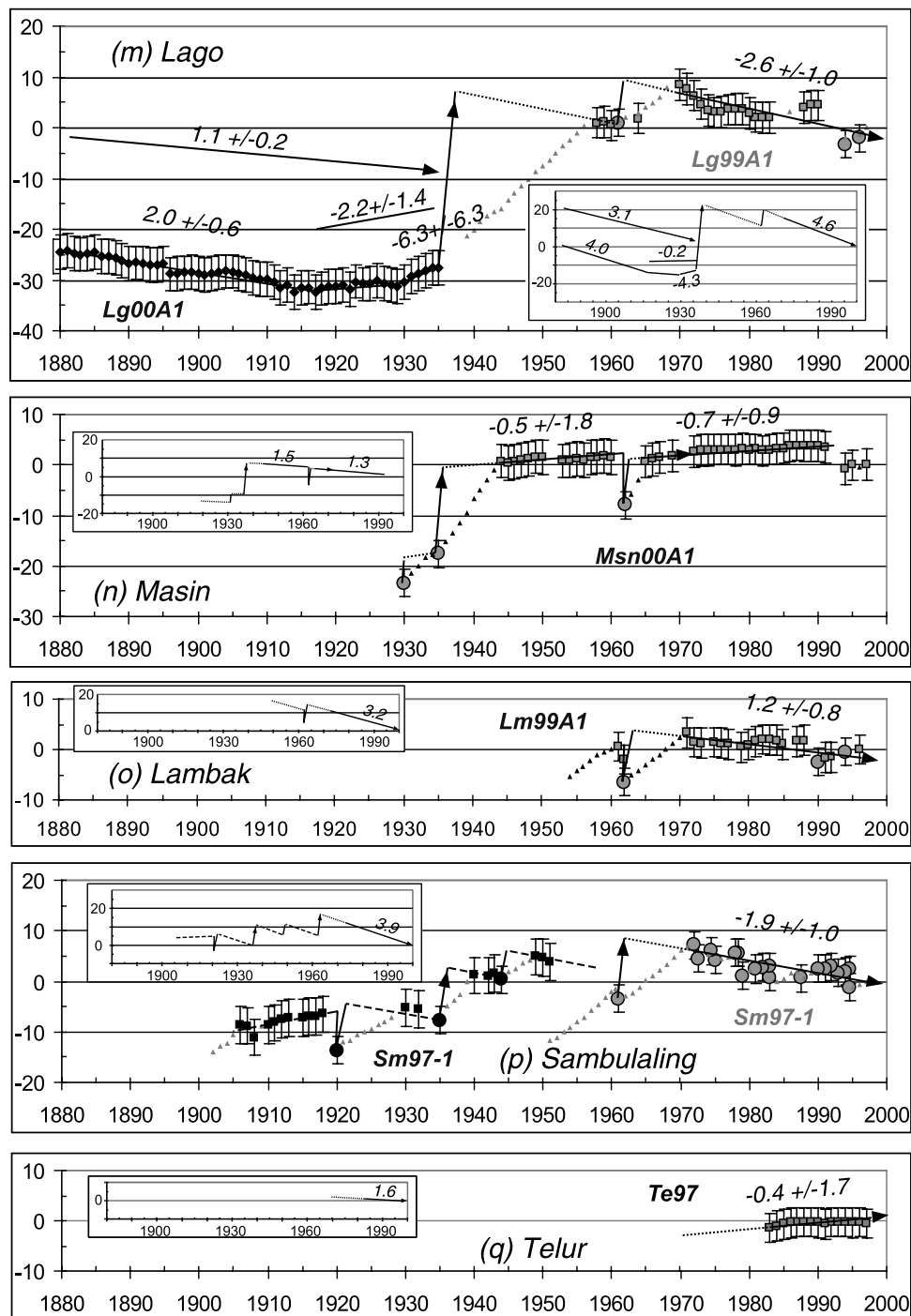
Figure 12. (continued)

must be considered first before assessment of its tectonic component.

[64] On the basis of surveys we conducted on reefs near 3°S, variation of HLS elevation within a single *Porites* coral microatolls are on average about ±2.6 cm (2σ) [*Zachariassen et al.*, 2000; this study]. The variation of average HLS elevations between microatolls from the same site is about ±5 cm (2σ). Hence, at those sites where we use more than one head to construct a record, as we have

done to measure sudden emergence in 1935 at Bendera (Figure 7), we must allow for uncertainties of this magnitude. Thus, in general, we cannot expect to resolve tectonic events that produce signals less than or equal to about 5 cm.

[65] Broad climatic regional events or oceanographically induced fluctuations in HLS are also nontectonic and must be assessed. One might expect these to resemble tectonic events, because they could produce spatially and temporally

coherent signals. Our records show, however, that even the most severe El Nino-Southern Oscillation (ENSO) and Indian Ocean Dipole (IOD) events, in 1997, 1994, 1986/7, and 1982/3 [*Saji et al.*, 1999] lowered HLS by generally no more than a few centimeters [*Natawidjaja*, 2003]. Most of these die-downs recover by upward growth to prior levels within just a few years. To further distinguish these regional climatic events from tectonic signals, we found that they produce geographically incoherent patterns [*Natawidjaja*, 2003].

[66] At several sites, nontectonic die-downs of up to a few centimeters occurred in years not associated with the known extreme climatic events. At a few sites, several-centimeter HLS drops may be associated with local tectonic causes. Drops of about 4 and 5 cm at Masin and Lambak in about 1991 (Figures 12n and 12o) could be related to an M_w 5.2 earthquake event that year (Figure 2). A 5 cm HLS drop in the early 1990s at Lago (Figure 12m) might also have been associated with this event. A 10 cm drop in HLS at Pono in 1986 (Figure 12e), which was not followed by recovery, was probably related to a nearby M 7.1 earthquake in 1984 [*Rivera et al.*, 2002]. Delay in die-down is plausible, as *Taylor et al.* [1987] have shown that for small uplifts an HLS die-down can lag one year or more behind the event, because a subsequent very low lowest annual tide may not occur more often than every several years.

[67] To quantify uncertainties in tectonic signals due to nontectonic fluctuations, we examine our three best-preserved HLS records of the past 30 years [*Natawidjaja*, 2003]. We do not present the detailed analysis here, but the result for the average value of the fluctuations is about ±2.7 cm (2-σ deviation). So, in Figure 12 all uneroded or preserved HLS points (the large filled circles) appear with an error bar of this magnitude.

2.2.2.2. Ambiguities Due to Erosion

[68] In the preceding sections, we took care to use a different symbol for the elevation of preserved HLS clips than we used for eroded HLS elevations (filled circles versus horizontal bars). As discussed in the preceding paragraphs, a 2-σ error of ±2.7 cm can be assigned to all of the uneroded HLS elevations. However, eroded points must bear errors that include this value plus an estimate of the amount of erosion. How do we assign these errors?

[69] A pristine microatoll has an upper surface ornamented by alternating concentric ridges and swales (e.g., Figure 13). These reflect the natural, nontectonic variability of annual lowest low tides. Swales and ridges represent years of HLS die-downs and unimpeded upward growth respectively. We have found that the amplitude of this microtopography usually is between 2 and 4 cm. Similar magnitudes of microtopography are common on heads in Vanuatu [*Taylor et al.*, 1987] and in the Cocos Islands [*Smithers and Woodroffe*, 2000]. More often than not, however, these concentric bands are either subdued or absent, due to erosion. Erosion thus adds an additional level of uncertainty in interpreting the HLS record.

[70] If erosion occurs predominantly as a diffusive process, then degradation will occur as illustrated in Figure 14. In this example we start in the upper panel with the actual slab of a young coral head from Sambulaling Island. Proceeding successively through lower panels, the ridges erode more rapidly than the swales, because of their

Figure 13. These heads at Angsa Island show largely uneroded concentric ridges and swales on their dead, upper surfaces, indicating little or no erosion.

more exposed position and greater ratio of surface area to volume.

[71] Since the amplitude of the microtopography of a head is 2 to 4 cm, 1 cm of erosion of the ridges will subdue but not eliminate the microtopography, and the HLS clips, buried beneath the swales, will remain uneroded (Figure 14, Stage 1). If concentric rings are barely apparent on the surface of the head, but HLS clips are still visible, then erosion of 2 to 4 cm has probably occurred (Figure 14, Stage 2). If no expression of concentric rings exists and HLS clips are not preserved, then erosion has probably equaled or exceeded 3 or 4 cm.

[72] We use this analysis in assigning errors to each of the HLS records in Figure 12. The total error is calculated as a function of the inherent fluctuation of HLS (±2.7 cm) and the estimated amount of erosion that the head has sustained, according to this formula:

$$\sigma_{HLS} = \pm\sqrt{(\sigma_{ol}^2 + \sigma_e^2)},$$

where σ_{ol} is the standard deviation of HLS fluctuations due to regional oceanographic and local causes (i.e., 2.7 cm), and σ_e is half of the estimated amount of erosion. The observed elevation of the eroded HLS is also corrected by the estimated amount of erosion.

2.2.3. Determination of Submergence and Emergence Rates

[73] To isolate large tectonic signals in the HLS records, we eliminate uncorrelated fluctuations, which are commonly small in amplitude and duration. We ignore them by calculating rates of change in HLS averaged over a decade or more (Figure 12). Since the uncertainties are not necessarily the same for each point in an HLS time series, the rates shown in Figure 12 are calculated from the best least squares fits to the weighted data.

[74] In Figure 12, average rates calculated over longer periods appear alongside sloping arrows above the data. Average rates calculated over shorter periods appear directly above solid lines drawn through the data. Dashed lines through the data indicate that the calculated rates are less
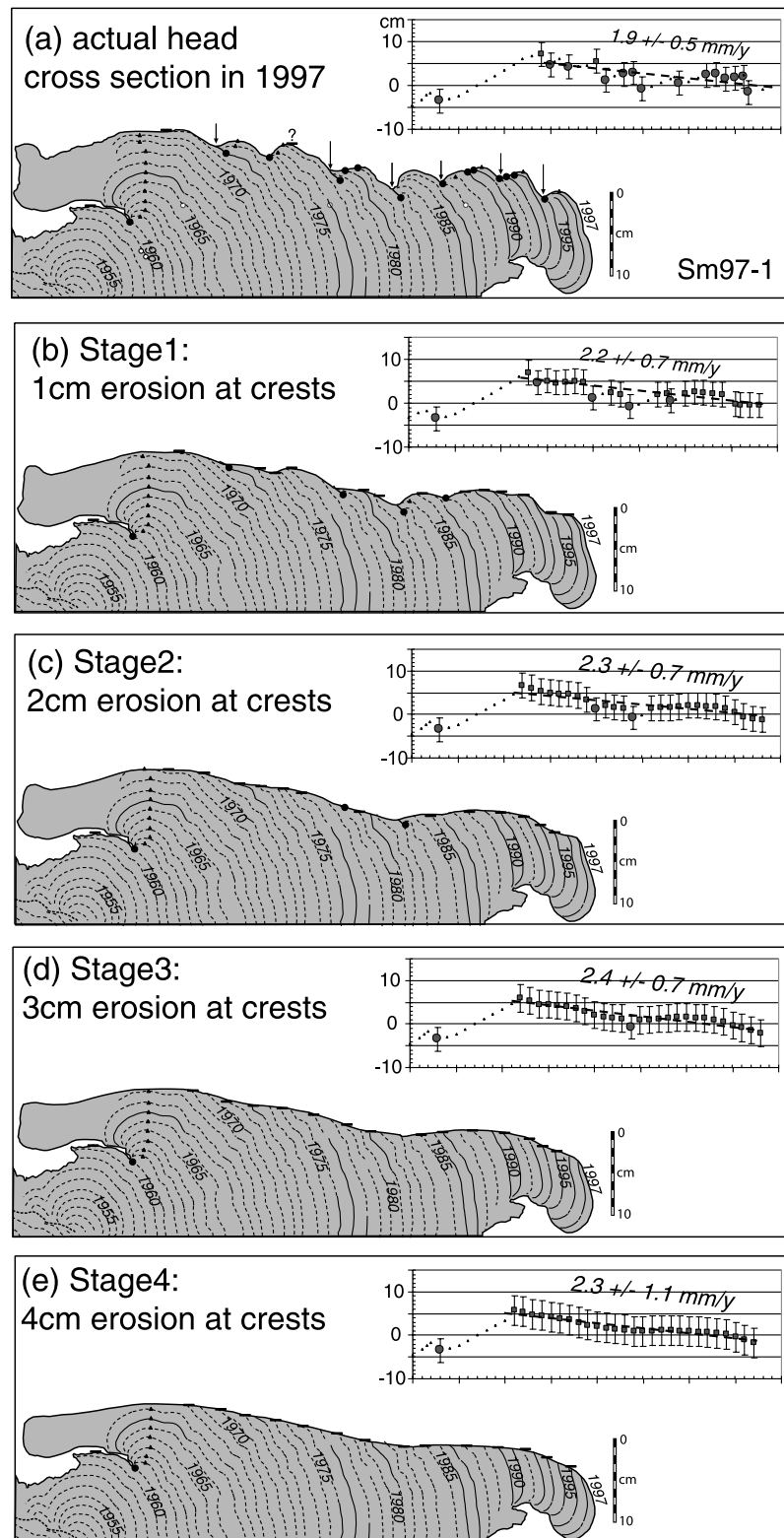
Figure 14. Erosion adds additional uncertainty to the rate calculations. These five figures show a hypothetical degradation of a coral surface assuming erosion occurs predominantly as a diffusive process. The ridges erode more rapidly than swales, because of their more exposed position and greater ratio of surface area to volume. Inset figures illustrate graphical representations of coral degradations, showing that the assigned uncertainties of the 2-σ HLS records are proportional to the severity of erosion.

certain, and dotted lines indicate rates that are extrapolated into periods lacking data.

[75] In the following sections, we will analyze tectonic signals recorded by coral microatolls. First, we discuss the most prominent signature: the 1935 event. Then, we discuss the second largest signal: the 1962 event(s). Finally, we discuss records of slow deformation before and after these events.

2.3. The 1935 Event

[76] Historical evidence of the 1935 earthquake is sparse. Below is the only set of field observations that have been published [*Berlage Jr.*, 1936]:

> A heavy earthquake hit the Batu islands in December 28; 09:06.83. Reports were received from Northern and Southern Sumatra. The person in charge of the lighthouse on the little island of Bodjo reported that the hill, on which the 60 m high light house stands, showed tears. Damage dimmed the light. Some walls of buildings next to the lighthouse cracked and roof tiles fell down, injuring two people. On Tello Island several residential houses collapsed, a number of people therein were hurt, and some were seriously injured. The "person in charge" of the Batu Islands mentioned later that the islands Tanabala and Sigata seem to have risen a little bit, since a reef fields that used to be flooded at high tide, now remain dry. The coastal lights of Sigata and Moeara Siberoet were lightly damaged. On Sumatra the earthquake was also very strong. In the area of Padang the local phone lines were broken. Several walls cracked. Trees, telephone poles and light poles, and also the wires, moved. In several residential houses and shop, glasses fell down. In the Oranje hotel plaster fell down, while behind the main building an electrical cable snapped. In several parts of the city the light system broke. In the pool the water was moving around and flooded the edge of the pool. Cars were difficult to control and bounced across the road. In Sibolga some houses collapsed. However, no person was injured. Strangely enough the chief of the village of Moearakoeang in the residence of Palembang reported that on December 28 there were "flood waves" seen on the river Ogan "while there was no earthquake". The epicenter of the earthquake was registered world-wide and was located about 0.3°S, 97.9°E, just west of the Batu islands. A great number of aftershocks followed.

[77] The Batu Islands comprise the islands of Tanabala, Tanamasa, Pini and other neighboring smaller islands. See Figure 3 for location of the islands Bodjo (now spelled "Bojo"), Tello, Tanabala and Sigata. "Reef fields" refers to an intertidal reef.

[78] We did not find a historical report on tsunami that might be associated with this event. However, we observed and mapped many reef blocks and debris in intertidal reef flats in this region that were probably associated with this event. Local people that we interviewed during our fieldwork in 1999 and in 2000 tell stories that support this hypothesis. One example is a middle-aged person at Barogang site who said that his father, who was about 10 years old in 1935, had told him a story about a big wave that struck the shore near their village then.

[79] Nine of our paleogeodetic sites show clear evidence of vertical deformation in about 1935 (Figures 12a, 12b, 12c, 12d, 12e, 12i, 12j, 12m, 12n, and 12p). The pattern of deformation is consistent with the historical notes above. It shows that the three sites closest to the trench emerged, whereas all sites closer to the mainland submerged (Figure 15b). Emergence of nearly a meter occurred at Bendera, about 100 km from the trench. Badgugu and Barogang experienced lesser emergences. The site with

the greatest submergence, 34 cm, is Lago, about 140 km from the trench axis and about 25 km above the subduction interface. The domains of emergence and submergence join along a line that is approximately 114 km from the trench axis but not quite parallel to it (Figure 15b). The geographic extent and magnitude of this deformation constrain the dimensions of rupture that produced the pattern, in particular its downdip limit and the magnitude of slip.

[80] We use the date of the 1935 event to ascertain the reliability of our visual ring counting and U-Th dates. We then discuss how we measured the values of uplift and submergence at the nine sites that record the event. After that, we compare our data with the model based on source parameters obtained by the seismologic study of *Rivera et al.* [2002]. Finally, we use elastic dislocation theory to estimate the source parameters of the event based solely on the paleogeodetic records.

2.3.1. Dating of the Event

[81] We have eight slabs from microatolls that were growing prior to the event, experienced it, but survived until the late 1990s. In each case, visual counting of annual bands inward from the outer surface of the slab yields a date for the event in the 1930s (Figure 16a). Uncertainties in counting range from 1 to 7 years, and the weighted average date for the event is 1935.5 ± 0.6. However, our convention is to assign the beginning of a growth year to the beginning of the darker band of the annual dark/light pair. This means that the beginning of our growth year is in about March, the beginning of the annual dry season. Thus we must add about 2 months to the growth-year date to derive a calendar date of 1935.8 ± 0.6. The slab count with the least uncertainty gives a date centered on 1936. This strongly suggests that the deformation is related to the large earthquake (M_w 7.7) of 28 December 1935.

[82] Twenty-three dates from U-Th analysis of the slabs also constrain the date of the event (Figure 16b). The discrepancy between dates from U-Th analysis and those from visual ring-counting is generally less than 5 years and usually within the analytical precision of the U-Th analyses. The weighted average date of the event, based on the U-Th dates, alone, is 1935 ± 1.2. The difference between the results of the two methods is therefore insignificant (-0.8 ± 1.2 years, 2σ).

2.3.2. Magnitude and Pattern of Vertical Deformation

[83] Measuring the vertical deformation associated with the 1935 earthquake would be rather straightforward if all one had to do were to subtract HLS values recorded immediately before and after the event. However, we must also use uncertainties in these values to determine uncertainties in the magnitude of deformation. We must also, in most cases, extrapolate from older and younger HLS clips to estimate the HLS values just before and after the earthquake.

[84] If the same head contains an HLS record for the periods both before and after the event, then we begin with the nearest data points both before and after the event. If these data points were recorded near the time of the earthquake, then using the long-term submergence or emergence rate to extrapolate values just before and after the earthquake is inconsequential.

[85] We particularly need to extrapolate to 1935 at sites where large submergence occurred. Since the coral grows
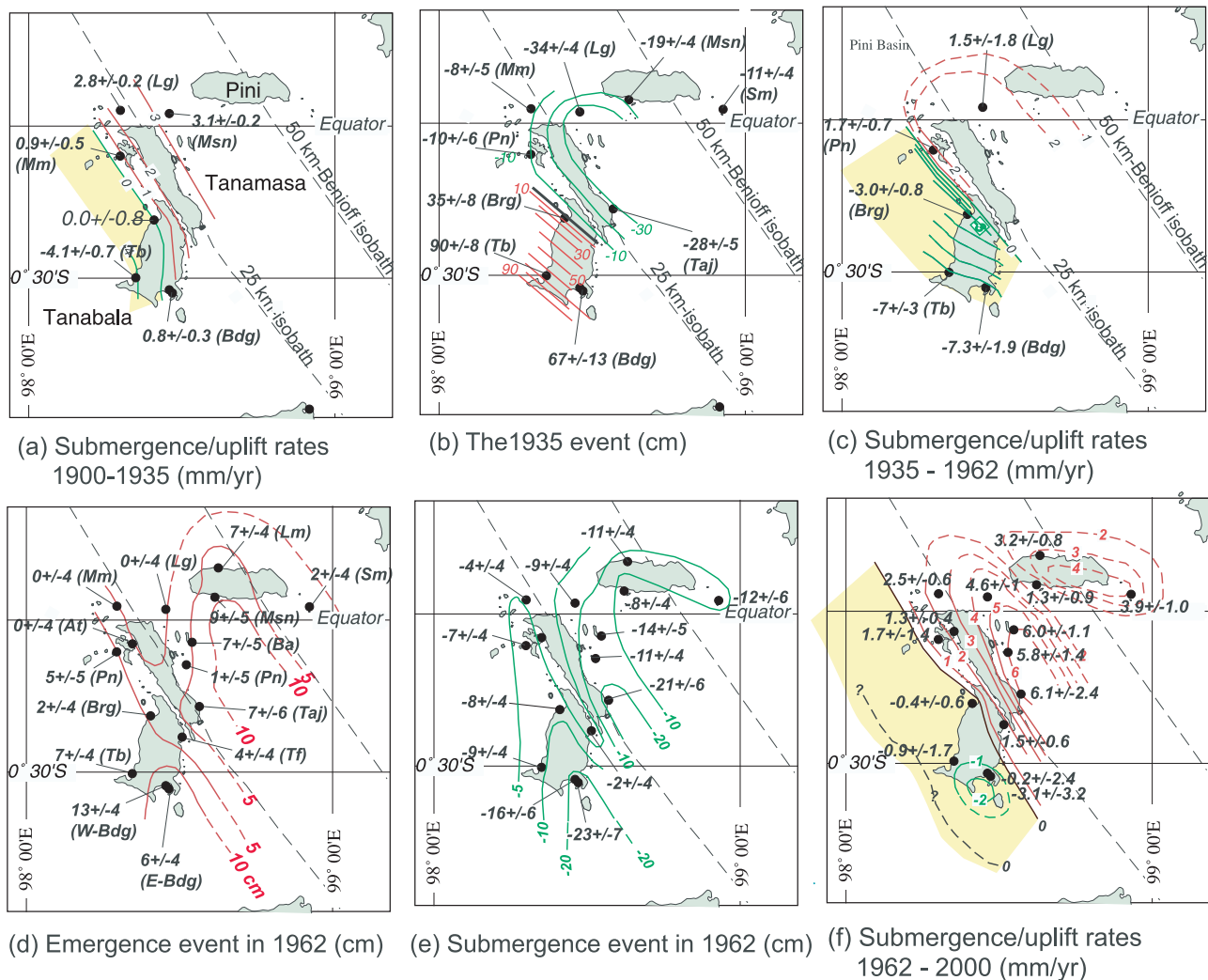
(a) Submergence/uplift rates 1900-1935 (mm/yr)

(b) The 1935 event (cm)

(c) Submergence/uplift rates 1935 - 1962 (mm/yr)

(d) Emergence event in 1962 (cm)

(e) Submergence event in 1962 (cm)

(f) Submergence/uplift rates 1962 - 2000 (mm/yr)

Figure 15. Summary of paleogeodetic records of vertical deformation for the twentieth century. Positive and negative values indicate uplift and submergence respectively. The large western islands were tilting southwestward in the decades prior to 1935 (a), between 1935 and 1962 (c), and after 1962 (f). Yellow patches indicate the area of submergence during the interseismic periods. During the 1935 event (b) the islands tilted northeastward; emergence occurred in the west (red contours), and submergence in the east (green contours). The 1962 emergence data (d) are contourable, but their cause maybe tectonic or climatic. The 1962 submergence event has a much larger magnitude than a signal that can be attributed to nontectonic sources. Therefore it likely represents a large aseismic slip event on the subduction interface outboard of the islands (e). Note that the sense of vertical motion during the interseismic periods is opposite that of the 1935 earthquake, and that the submergence/uplift rates differ significantly between the three periods separated by the 1935 and 1962 events. Submergence rates were fastest in the post-earthquake period 1935–1962 and slowest in the past four decades. These differences indicate changes in slip rates and other processes operating on and around the subduction interface.

upward at rates of only about 1 cm/yr, a submergence of many centimeters will require many years of free upward growth before the head again reaches the HLS. Thus post-earthquake periods devoid of HLS clips tend to be about as many years long as the submergence (in centimeters) (e.g., Figures 12f, 12i, 12j, 12m, 12n, and 12p). Lago, where submergence was greatest, provides the most extreme example. Figure 12m shows that no HLS clips occurred until about 22 years after the event. In this and other cases, extrapolation of the most proximal HLS clip back to 1935,

using the average rate of submergence or emergence, influences the magnitude of the 1935 step by a few centimeters or less.

[86] At Bendera and Badgugu, the HLS histories are composites assembled from more than one head. Emergence elevated some of the heads so much that they died. Heads that were growing well below lowest low tide survived the event and recorded the post-1935 HLS history. In these two cases, we must also include inter-head uncertainties in HLS, which are about ±5 cm. Thus the total
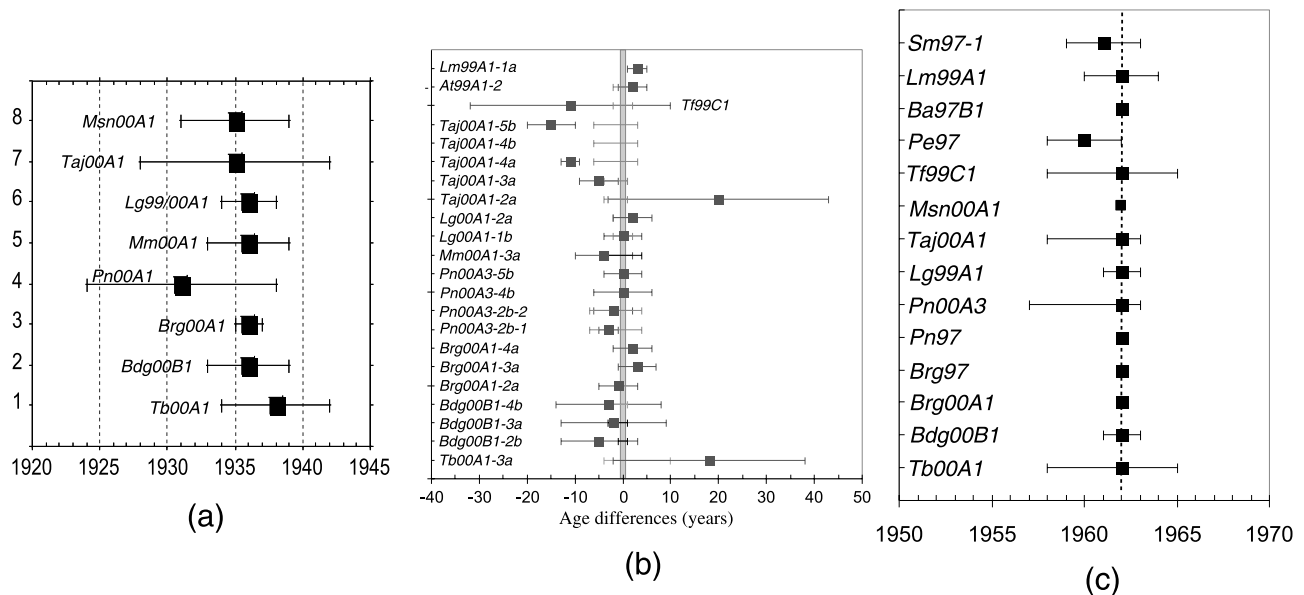
Figure 16. Dates of events based on visual ring counting and U-Th analysis. (a) Date ranges of the December 1935 event based on visual ring counting from the modern exterior ring. The weighted average of the dates is 1935.8 ± 0.6 (2σ). (b) Comparison of the U-Th dates and their 2σ uncertainties (squares and bars) with the assigned dates from visual ring counting. (c) Date ranges for the 1962 event based on visual ring counting.

uncertainty, a combination of the intra head uncertainty in the preserved HLS (i.e., ±2.7 cm) and the inter head HLS variation, is this:

$$\sigma_{ol(inter-head)} = \pm\sqrt{(2.7^2 + 5^2)}cm = \pm5.7 \ cm(2\sigma).$$

[87] Note that the solid, dashed, or dotted lines through the data in Figure 12 indicate averaged rates of vertical deformation, not the actual extrapolations used to calculate the magnitude of submergence and emergence for the 1935 event. The actual calculation uses the least squares average rates shown in Figure 12, but we extrapolated to 1935 from the point of the closest HLS clip to the event.

[88] The coral microatoll has an odd "response spectrum." If emergence is approximately equal to the diurnal tidal fluctuations at spring tides (that is, about 1.5 m), most of the coseismic step should be recorded within a half day, since even at neap tides the head would be out of the water at least 75 cm right after the earthquake. If emergence is only about half of the magnitude of spring tides, then emergence might not begin to be recorded for as much as a week after the event, until the next spring tide produced the monthly lowest tides. The full extent of coseismic emergence, however, might not be recorded for as much as a year, since annual lowest low tides typically occur only in June, July or August. Thus all but a few effects of the coseismic emergence would have appeared within a week or two at Bendera and Badgugu, where emergence was about 90 and 66 cm. Smaller emergences, of the order of 10 or 20 cm, might have appeared in the HLS record later; most likely within the next few years, since our records show that extreme annual lowest low tides vary by only a few centimeters and occur every few years. The fact that HLS was recorded within a year at all of our emergent sites (Figure 12) demonstrates that this analysis is fundamentally

correct, and that only post-seismic transients that occurred within about a year after the earthquake would be hidden within the "coseismic" signal.

[89] The submergence records of the 1935 event constrain post-seismic transients much more poorly. As Figure 12 shows, post-seismic periods ranging from 5 to 40 years contain no HLS clips.

[90] In summary, the principal constraints provided by the paleogeodetic data for the 1935 event are these:

[91] 1. A domain of emergence occurred outboard of about the 25 km isobath of the subduction interface (Figure 15b). Values of emergence increase systematically southwestward, toward the trench. The highest emergence was at Bendera (90 cm).

[92] 2. A domain of submergence appears inboard of the same line. The magnitude of submergence is greatest at Lago (34 cm), about 10 km northeast of the 25 km isobath, and diminishes gradually toward the mainland.

[93] 3. The hinge line separating domains of emergence and submergence runs near the western coast of Tanamasa Island. The best fit hinge line strikes about N 41°W, several degrees more westerly than the trench, about 115 km to the southwest. This suggests that the event involved a small component of right-lateral slip on the subjacent subduction interface.

2.3.3. Comparison of Paleogeodetic and Seismologic Source Models

[94] We can employ elastic dislocation modeling to constrain further the parameters of fault rupture in the earthquake. *Rivera et al.* [2002] have already attempted this, but with a completely independent data set. They used old historical seismograms of the 1935 event from four stations: De Bilt, Wellington, College, and Honolulu to constrain the source parameters of the earthquake. Rivera et al. estimate the seismic moment of the 1935 event to be
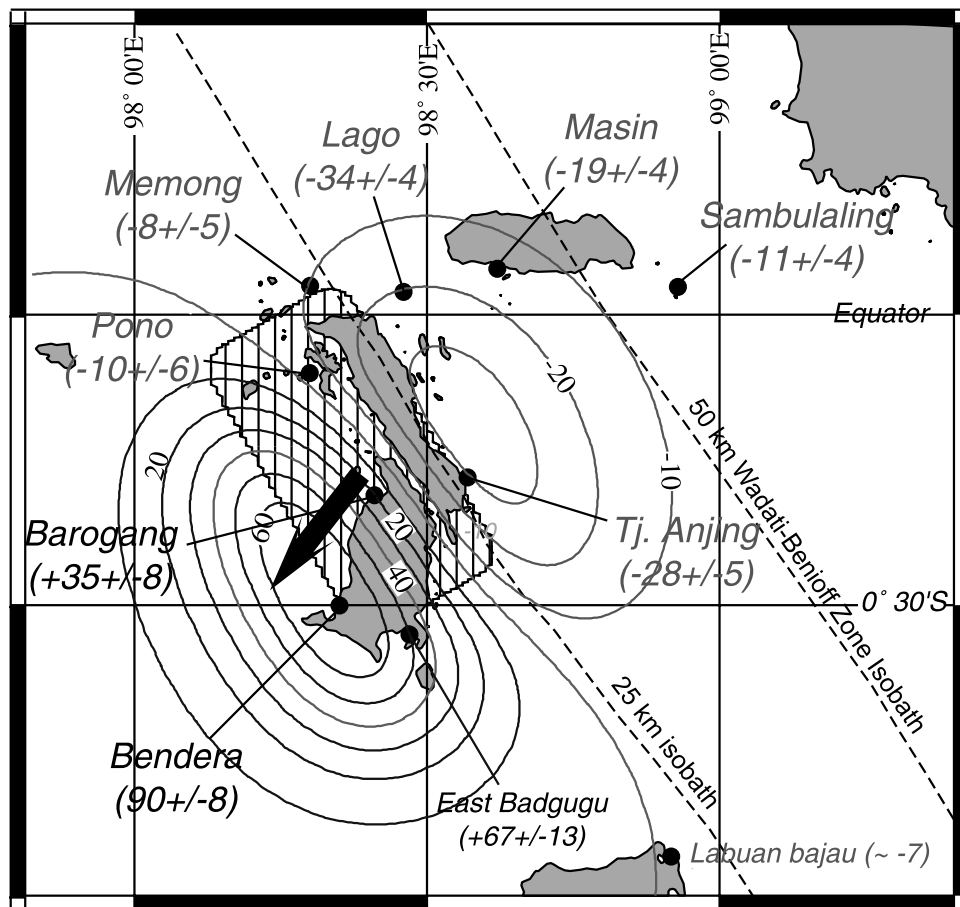
Figure 17. A comparison of vertical deformation for the 1935 event. Values, in centimeters, plotted under site names are from analysis of our microatoll records. Contours are from elastic dislocation model derived from seismologic rupture parameters from *Rivera et al.* [2002]. The striped rectangle is the seismologically determined source in plan view, and the black arrow represents the azimuth of the slip vector. The seismologic source model uses a uniform value of 3 m slip across the rectangular source.

3.3×10^{20} N m ($M_w = 7.7$). Furthermore, based on a shorter and higher source time-function recorded on the seismogram at Wellington, they conclude that rupture propagation was unidirectional toward the southeast. Thus, assuming a rupture velocity of 2.0–2.5 km/s for the 30-s rupture, they estimate a rupture length of 60 to 70 km (Figure 17). Assuming a standard 2:1 ratio for strike length to dip length [*Kanamori and Anderson*, 1975], they then calculate an average displacement of about 3 m. Of course this seismic source model is not a unique solution. Another solution, for example, might assume a 4:1 ratio for strike to dip length and hence calculate an average coseismic slip twice as great. Nonetheless, from their estimates of source parameters, *Rivera et al.* [2002] used elastic dislocation theory to estimate the pattern of vertical deformation. They calculate elliptical uplift and submergence regions, with peak amplitudes of about 70 and 35 cm, respectively (Figure 17). A minor right-lateral component of slip yields a hingeline between the two domains that is slightly oblique to the strike of the subduction interface.

[95] It is interesting to compare this model of vertical deformation with our paleogeodetic data. To first order, the model from the historical seismic data is consistent with the paleogeodetic data (Figure 17). The locations and magni-

tude of emergence and submergence are similar, as are the hingelines between emergence and submergence. The principal difference between the seismologically derived model and the paleogeodetic data is in the magnitude of deformation. Figure 17 shows that, with the exception of the values at Pono, the paleogeodetic values of emergence and submergence range from about 35 to 70% greater than the model values. Since the moment magnitude chosen for the model by *Rivera et al.* [2002] is near the upper end of their range of plausible values, it is possible that this difference is significant. Perhaps, the difference reflects significant postseismic slip on the subduction interface within a year of the earthquake.

2.4. The 1962 Event

[96] Now we will analyze data related to the event of 1962. This event consisted of an emergence event followed by a submergence event. It is not associated with any large earthquake; therefore we consider it to be an aseismic rupture.

[97] The time of the event is well constrained by visual ring counting to have occurred during the first half of that year (Figure 16c). The magnitude and extent of the deformation is greater than what could have been produced during a few

small (*M* 6 or less) earthquakes that occurred in the region in 1961 and 1962 (Figure 2). More probably, the moderate earthquakes were a minor seismic manifestation of whatever caused this much larger aseismic event.

[98] Most of the sites reveal that the 1962 episode comprises two consecutive geodetic events; the first characterized by emergence of the sites and the second by their submergence. In both episodes, the magnitude of vertical deformation is a few times less than that of the 1935 event. Thus one would expect that if the source of the 1962 events were the subduction interface, the slip on the interface would have been much less than it was in 1935; perhaps, the slip in 1962 was just several tens of centimeters.

[99] At most sites, the magnitude of the initial emergence is smaller than that of the subsequent submergence. This fact manifests itself in many of the records as a distinct step up in HLS elevations after 1962 (in particular, Figures 12b, 12d, 12e, 12j, 12l, 12m, and 12p). In addition to the distinctly higher HLS after 1962, at many sites the long-term rate of emergence or submergence changed appreciably at the time of the event (Figures 12a, 12c, 12d, 12j, and 12m).

[100] Records from sites where the magnitude of the 1962 episode is small constrain the duration of the episode best, because the time required for the living perimeters to grow back up to HLS was short. The Masin site may provide our best constraint on the duration of the submergence event. It clearly indicates that the 1962 submergence event ended there no later than 1964 (Figure 12n). The record from Tofa (12f) suggests a similarly short duration, but it is more ambiguous. On the basis of the record from these two sites, we think that the entire episode took place in less than two years.

[101] Maps of deformation during both the emergence and submergence events show fairly distinct, contourable patterns. The emergence event appears to consist of two northwest trending ridges, each a little over 10 cm high and separated by a swale of lesser uplift (Figure 15d). The swale between the two ridges is very close to the hinge line of the deformation in 1935. If this deformation resulted from slip on the subduction interface, then the ridges might be evidence for slip on the lower portion of the 1935 rupture and on a patch downdip from it. The swale suggests that these two patches were distinct, with minimal if any overlap.

[102] The occurrence of strong ENSO and IOD events in 1962 [*Saji et al.*, 1999] is, however, reason to be cautious in interpreting this emergence event as being of tectonic origin. The magnitude of die-downs during the strongest ENSO and IOD events of the past two decades, in 1982, 1986, 1994, and 1997 are commonly up to 3 cm in the HLS records, but in some cases are close to 10 cm [*Natawidjaja*, 2003]. Thus die-downs of a few centimeters associated with the strong ENSO/IOD climatic event of 1962 probably contaminate the tectonic signal. Still, the fact that the emergence in 1962 appears to have a pattern and magnitudes greater than those commonly produced by the ENSO/IOD events suggests that it is predominantly tectonic in origin.

[103] The deformation pattern of the subsequent submergence event is nearly a mirror image of the preceding emergence (Figure 15e). It consists of two northwest-trending synclinal troughs, separated by a long, narrow region of minimal submergence. The synclinal axes appear to be in the same locations as the anticlinal crests of the prior emergence event. Furthermore, the location of the ridge between the zones of submergence is indistinguishable from the swale between the anticlinal ridges of the preceding emergence event. These coincidences suggest that slip during the submergence event was on parts of the subduction interface adjacent to those patches that slipped in the emergence event. In this interpretation, the two slip patches that produced the submergence event would be immediately updip from the two slip patches that produced the emergence event.

[104] The submergence event of 1962 also appears to have an odd extension that bends northward and eastward through Pini Island. We could interpret this as northwest directed slip on the subduction interface. However, our data poorly constrain this sector of the submergence event, so we are not eager to speculate further about this part of the signal.

2.5. Deformation in the Intervening Decades

[105] Although the rapid 1935 and 1962 events are prominent in the paleogeodetic records of Sumatran subduction, evidence of slow vertical deformation throughout most of the twentieth century is also ubiquitous among the outer-arc islands. Generally, sites experienced slow vertical deformation opposite in sense to their co-seismic deformation in 1935. That is, places that submerged suddenly in 1935 emerged slowly throughout the rest of the century, and conversely, sites that emerged suddenly in 1935 submerged slowly during the remainder of the century. Basically, this suggests an interplay between slow strain accumulation and sudden strain relief, as has been suggested for other subduction zones (e.g., Nankai trough, Japan [*Thatcher*, 1984a] and Alaska [*Plafker*, 1965; *Savage and Plafker*, 1991]. In detail, however, the patterns of vertical deformation during the three periods separated by the 1935 and 1962 events differ substantially from each other. These differences indicate decadal variability in the processes operating on and around the subduction interface, and that the 1935 and 1962 events affected subduction processes significantly.

2.5.1. Correction for Global Hydroisostatic Rise in Sea Level

[106] Before we can analyze the tectonic rates of deformation in our paleogeodetic records, a global-sea-level-rise effect must be removed. Rates of sea level rise, determined from tide-gauge stations throughout the world, range from about 1.0 to 2.4 mm/yr [e.g., *Barnett*, 1984; *Gornitz et al.*, 1982; *Peltier and Tushingham*, 1991]. This rise has been occurring for at least the past eight decades, but is less certain for the earlier part of the twentieth century. It is believed to be a consequence of global warming, which causes thermal expansion of the upper layers of the ocean and melting of the glacial ice [*Barnett*, 1984; *Peltier and Tushingham*, 1989]. Clearly, our paleogeodetic records of the twentieth century would include this nontectonic submergence. Hence this signal needs to be removed prior to an analysis of tectonic components.

[107] In the case of a submerging site, the effect will be to reduce the rate of submergence by 1 to 2 mm/yr. For example, the 6.1 mm/yr rate at Bendera (Figure 12a) would be reduced to about 4 or 5 mm/yr (Figure 12a inset). For an

emerging site, however, the tectonic rate would be 1 to 2 mm/yr greater than the rate recorded in the microatoll. Thus the observed 4 mm/yr rate of emergence at Bai indicates a rate of tectonic uplift of 5 to 6 mm/yr (Figure 12l). Records that have been experiencing submergence at rates of only 1–2 mm actually indicate tectonic stability or even slight uplift. For example, when stripped of its global-sea-level-rise effect, the 0.5 mm/yr submergence at Tofa yields a tectonic uplift rate of 0.5 to 1.5 mm/yr (Figure 12f).

[108] In the inset graphs in each panel of Figure 12 we have applied an adjustment of 2 mm/yr to all of the records. However, an adjustment of 1 mm/yr is equally defensible, so we will consider this correction as well in our modeling of the data. In the following discussion we will use average rates of emergence and submergence that reflect a 2 mm/yr correction for a global sea level rise as shown in Figure 12 inset.

2.5.2. Dividing the Century Into Three Periods

[109] Most of the site records show that rates of slow vertical deformation have not been constant throughout the century. For example, at Bendera the average rate of submergence in the three decades prior to 1935 was about 4 mm/yr (Figure 12a). Within this period, decadal rates varied from as little as 1 mm/y to as much as 10 mm/yr. In the three decades between 1935 and 1961, the average rate was 7 mm/yr. In the four decades following 1962, the average rate of submergence was about 1 mm/yr. In fact, 1935 and 1962 demarcate natural divisions in the history of vertical deformation for more than half of the sites. We thus separate our discussion of the records into three periods, pre-1935, 1935 to 1962, and post-1962.

2.5.3. Decades Prior to 1935

[110] In the decades prior to 1935, all but the westernmost site were rising (Figure 15a). Lago, the site with the greatest measured submergence in 1935, was experiencing the highest rate of uplift, 3 mm/yr. Bendera, the site with the greatest measured emergence in 1935, was experiencing the fastest subsidence, 4 mm/yr. The hingeline between uplift and submergence ran parallel to the subduction isobaths, except in the southern part of the area, where it turned north-south. The rate of tilt in the submerging region was lower than in the region of emergence. Use of a 1 mm/yr correction, rather than 2 mm/yr, would shift the hingeline 5 km or so northeastward, toward the mainland. In either the 1 or the 2 mm/yr case, the hingeline is rather close to the hingeline of the 1935 event in the north, but deviates tens of kilometers westward from the 1935 hinge in the south.

[111] A few of the records contain clear evidence for changes in rates that are precursory to the 1935 earthquake (Figures 12a, 12b, 12i, and 12m). Submergence at Bendera, for example, accelerated from about 1 to 8 mm/yr. The rate of emergence at Memong slowed from about 3.3 mm/yr to near zero. At Lago, emergence of about 4 mm/yr switched to submergence of about 4 mm/yr. These changes in the few years prior to the 1935 earthquake hint at changes in the rate of slip on the subduction interface just before seismic failure of the interface.

2.5.4. Decades Between 1935 and 1961

[112] The pattern of post-1935 rates is grossly similar to the pre-1935 pattern (cf. Figures 15c and 15a). After the earthquake, tilting toward the southwest continued to predominate. However, post-1935 rates of submergence are nearly double the pre-1935 rates. Another difference is the markedly higher rate of tilt across the northeastern third of Tanabala Island, near the hingeline, than to the southwest. Moreover, the deviation of contours apparent before 1935 in the southern part of the region is absent in the post-1935 period.

[113] Post-1935 vertical deformation in the region of large coseismic submergence, northeast of Tanamasa Island, are unrecoverable, because most of the microatolls took more than a decade to grow up to their new HLS level. Nonetheless, contouring of submergence rates in the surrounding regions suggests that this region was sustaining tectonic emergence in the decades after the earthquake.

[114] It is also important to note that the post-1935 data reveal few if any changes in rate in the two and a half decades after the earthquake. Thus a viscous response to the coseismic rupture and redistribution of stresses seems to be absent. All of the well-constrained sites show that the rate of deformation remained constant (Figure 12). The only exception to this may be at Barogang, where an immediately post-seismic rate of submergence of 6 mm/yr may gradually roll over into a 1.4 mm/yr rate of emergence by 1962 (Figure 12c). This record also suggests that the rate of submergence in the year or two after 1935 could have been as high as 13 mm/yr. This record may be significant, because it is one of only two good post-1935 records very close to the hingeline of the 1935 event. It suggests that rates of slip on the subduction interface may have varied between 1935 and 1962 near the downdip edge of the 1935 rupture. Nonetheless, this would have to be a very local effect along just a part of the hingeline, because the other record from near the hingeline, at Pono, does not indicate a similar transient. Since the Barogang record must be recording only a very local transient, we ignore it in the modeling efforts presented in the next section.

2.5.5. Decades Between 1962 and 2000

[115] This latest of the three interseismic periods contains the most complete record of vertical deformation. An HLS record for this latest period exists from almost all of our sites (Figure 12). In map view, the data show a pattern of deformation that is broadly similar to that of the previous interseismic periods—southwestward tilt of the islands (Figure 15f). However, there is a significant difference. The modern rate of submergence near the southwestern coast of Tanabala is a mere 1 to 2 mm/yr, rather than the 4 and 7 mm/yr rates documented for the pre- and post-1935 periods. The trend of the hingeline between regions of emergence and submergence is very well constrained to be parallel to the trench and the isobaths of the subduction interface. As for the post-1935 period, there is no clear indication of time-dependent changes in rate over the interval.

[116] Patterns within the area of emergence are also clearer than they are for the pre- and post-1935 periods. Two features stand out. First, very high emergence rates are occurring just off the east coast of Tanamasa. Although there are no data further east, except along the coast of Pini Island, we depict the uplift pattern as a northwest-plunging ridge of emergence. Second, another ridge is demarcated by the three sites on and near Pini Island. This feature is interesting because it is nearly parallel to the long axis of the Island, rather than parallel to the trench or outer-arc ridge.

2.6. Elastic Modeling

[117] Elastic dislocation models have been used frequently to explain the observed surface deformation above subduction zones. They appear to provide good explanations of the kinematic behaviors of subduction zones [*Kanamori*, 1973; *Savage*, 1983, 1995; *Thatcher*, 1984b; *Zachariasen et al.*, 2000]. We model deformation associated with the 1935 and the 1962 events as well as the inter-event slow deformations using a 2-D model, described by *Sieh et al.* [1999]. This model, illustrated in Figure 18, differs from the commonly used back-slip model of *Savage* [1983], in that it utilizes a dislocation surface below the subduction interface in addition to slip in the interface. This removes the need for the geologically implausible normal slip in the interface during interseismic periods. The geometry of the subduction interface in the model is defined by the location of the trench and the top of the Benioff-Wadati zone, based upon locations of seismic hypocenters from the relocated ISC: 1965–1998 [*Engdahl et al.*, 1998]. Modeling the 1935 and 1962 events, involves simply finding the best solutions for the location of the rupture patch and the associated slip on the subduction interface.

[118] For the three periods of interseismic deformation, the slab thickness in the model is arbitrarily set to 15 km thick at the trench, and it goes to zero at depth about 160 km, for reasons of mathematical convenience (Figure 18a). Modeling results are not sensitive to the assigned thickness of the slab because the interfaces at the top and the bottom of the slab produce signals that are nearly mirror images, and nearly cancel each another along most of the slab (Figure 18b). Setting the thickness at 30 km, for example, will give solutions nearly identical to those produced by the 15 km thick model. In the limit of a slab thickness of zero, slip on the top and bottom interfaces will exactly cancel each another, and the model will be identical to the commonly used back-slip model [*Savage*, 1983]. The convergence rate V_{plate} is fixed at 4 cm/yr as constrained by the GPS data and global plate models. That is, we fix the downdip portion of the interface to slip continuously at 4 cm/yr.

[119] The inversion, then, searches for the best fit to the three or four remaining free parameters: the depth below sea level of the updip tip of the principal locked zone (d_{lock}), the depth of the updip tip of the patch that is steadily slipping (d_{slip}), and the amount of slip on the different patches (Figure 18a). To reduce free parameters, we initially fix d_{slip} at 27 km depth, because this coincides with the downdip limit of rupture in 1935. However, if we cannot find a suitable fit to the data, we let d_{slip} vary.

2.6.1. Elastic Dislocation Model of the 1935 Event

[120] The paleogeodetic data associated with the 1935 event vary principally as a function of distance from the trench, or more precisely as a function of distance from the hingeline. A 2-D treatment of these data should suffice, since they vary little along strike. The results of our modeling are presented in Figure 19, panel B.

[121] Searching for the best model, we first projected the observed vertical deformations onto a cross section perpendicular to the average strike of the trench and isobaths. In this case, the paleoseismic data are moderately well fit by uniform slip of 2.5 m on a patch of the subduction interface 94 to 125 km downdip of the trench axis and 17 to 27 km deep [*Natawidjaja*, 2003]. These model parameters are
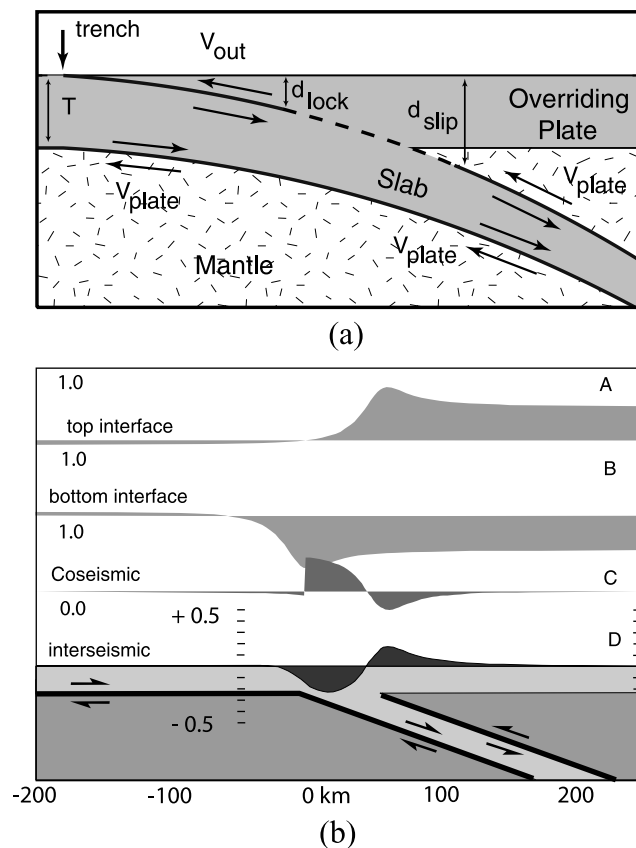

(a)

(b)

Figure 18. (a) Sketch showing the parameters of an idealized elastic dislocation model of deformation at a subduction zone. Dark lines are slipping interface. Dashed line is a locked patch or patch that slips during the event [after *Sieh et al.*, 1999]. (b) An elastic dislocation model of an earthquake cycle. Dark bold line is interface slips at the plate rate. Panels A and B show contributions to vertical motion from individual sources. Panel D shows the combined vertical motions from top and bottom of the slab. Note that motions due to slip on the top and the bottom interfaces are nearly mirror images of each other. So, in steady state subduction they nearly cancel one another. Panel C shows vertical motion during a seismic event, which nearly mirrors that of the interseismic period.

quite similar to those derived from the seismological study (Figure 17). However, the model underestimates the observed values at the three westernmost sites. We then attempted to reduce the misfit that might be due to the slight obliquity of the hingeline (as suggested by paleogeodetic data in Figure 15b) by projecting the data onto a cross section perpendicular to the hingeline rather than perpendicular to the trench (Figure 19, panel B). The location of the rupture in this model is about 88 to 125 km from the trench, 15 to 27 km deep. The magnitude of slip is a uniform 2.3 m. This model is an improvement, because two of the three westernmost points agree with the model deformation. However, the point at (Tb) is still misfit (by about 10 cm), and the point at Barogang (Brg) is fit at the very edge of its lower error limit. We probably could fit these points better without degrading the fit to the other points by adding an additional few tens of centimeters of slip to the upper half of
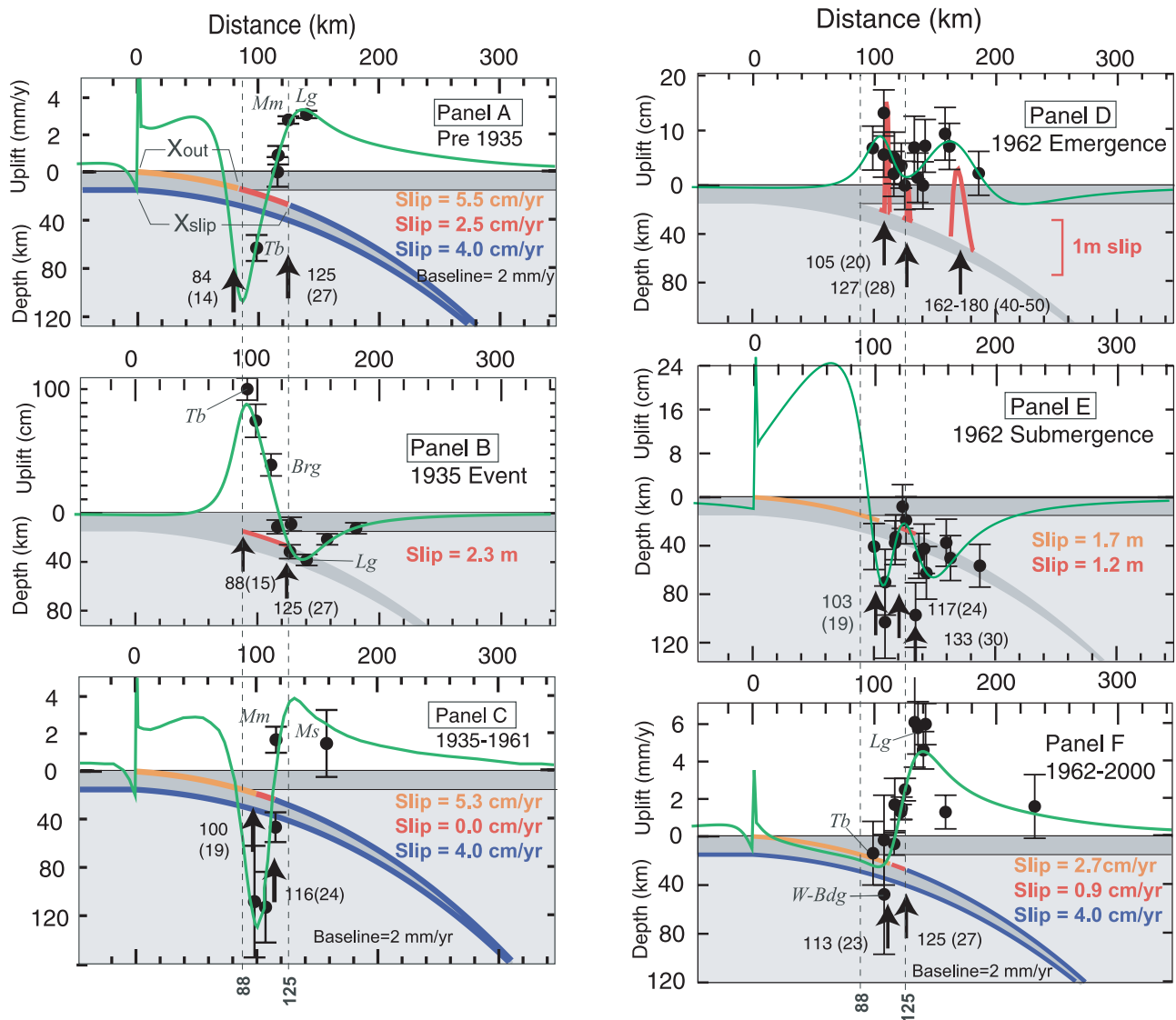
Figure 19. Summary of elastic dislocation models of the century-long paleogeodetic history. The black dots are uplift and submergence data derived the microatolls. The black bars represent 2σ uncertainties. The scale for these data appears on the upper part of the *y* axis of the plot. Note that the scale for data of the 1935 event in Figure 19b is different from the rest. The orange and/or the red patches represent the locations of slips on the interface. Blue lines represent stable sliding on the interface. The green line is the vertical deformation predicted by the inversion. The 1935 and the 1962 events dominate the history and demarcate appreciable changes in the behavior of the subduction interface. Figure 19a shows that the interface outboard of the islands (orange patch) may have been slipping at a rate slightly higher than the plate rate. The soon-to-fail patch (red) is slipping at about half the plate rate. Figure 19b illustrates that the paleogeodetic data can be well fit by 2.3 m of slip on the interface below the islands in 1935. After the 1935 rupture (Figure 19c), aseismic slip on the orange patch continued at a fast pace, but also extended downdip into the upper part of the 1935 rupture; the central part of the 1935 rupture was fully locked during this period. Figures 19d and 19e show that paleogeodetic signals of the 1962 event may reflect a large aseismic slip on local patches of the interface. Modeling of the modern paleogeodetic signals (Figure 19f) suggests that slip on the interface, outboard of the islands, has slowed to about half of the plate rate. The lower half of the 1935 patch may now be creeping at about 1 cm/yr.

the rupture patch. However, we have not actually developed this inhomogeneous slip model, nor we have attempted to take into account any post-seismic transient slip or visco-elastic responses that might have occurred in months following the event.

[122] In any case, the downdip extent of the rupture is tightly constrained by our data. The updip limit of the rupture is constrained less well. We could extend the updip edge of the rupture about 15 to 20 km trenchward without severely misfitting the data.

2.6.2. Elastic Dislocation Model of the 1962 Event

[123] To model the paleogeodetic emergence and submergence of 1962, we projected all the data onto a cross section perpendicular to the trench and interface isobaths. The maps of the data show clearly, however, that the data vary both as a function of distance from the trench and parallel to its strike. Thus our 2-D representation is only a starting point for understanding what happened during the 1962 episode.

2.6.2.1. The 1962 Emergence

[124] Paleogeodetic signals for the 1962 emergence event are barely larger than those produced by ENSO, and suggest only a weak geographic pattern. Nonetheless, assuming a tectonic origin, the inferred double-peaked emergence can be fairly well modeled by slips on three narrow strips along the interface (Figure 19, panel D). The two patches nearer the trench are located on the center of and near the downdip limit of the 1935 rupture. Slip on these patches reaches maxima of about 50 and 170 cm. The bigger patch, about 20 km wide is much deeper than the 1935 rupture. It occurs at a depth of about 45 km, about 170 km from the trench axis. Maximum slip on this patch is about 120 cm. Thus our model at least demonstrates that a tectonic hypothesis for the 1962 emergence is plausible. Even so, a nontectonic origin cannot be ruled out.

2.6.2.2. The 1962 Submergence

[125] The 1962 submergence event is significantly larger than the preceding emergence event. The paleogeodetic submergences generally do not recover in subsequent years. This strongly suggests a tectonic origin. Our model in Figure 19, panel E shows that uniform slips of 1.7 m on the interface between the trench and the islands and of 1.2 m on a patch near the downdip edge of the 1935 rupture produce the double-troughed deformation pattern. The model curve fits much of the data, but the two extreme submergence values are grossly misfit. These are the southernmost points in each trough. A 3-D model with slip increasing southward might provide a better fit of these maxima. The steady southeastward increase in submergence values supports this suggestion. The principal insights provided by this initial 2-D model are that a meter or two of slip is required on the interface outboard of the islands to explain submergence of the islands.

[126] Contamination by the 1962 ENSO/IOD event might account for as much as one-third to one half of the magnitude of the emergence event, so the slips associated with that event might have been smaller than we modeled. Nevertheless, even if this is the case, the 1962 aseismic episode has slips much larger than slips associated with rapid aseismic ruptures observed in Cascadia [*Dragert et al.*, 2001; *Miller et al.*, 2002], in Mexico [*Lowry et al.*, 2001], and in Japan [e.g., *Heki et al.*, 1997].

2.6.3. Elastic Modeling of Slow Deformation

2.6.3.1. Modeling of Deformation Rates Prior to 1935

[127] Figure 19a shows our best fitting model for the pattern of slow deformation recorded by the microatolls in the decades prior to 1935. We can find a good solution with a downdip limit of the locking equal to the downdip limit of failure in 1935 (125 km from the trench axis and $D_{slip} = 27$ km). Farther landward, slip on the interface is at the plate convergence rate of 40 mm/yr. With these two parameters fixed, the three free parameters are the location of the updip tip of the locked patch (D_{lock}), the rate of creep on the

interface outboard of the locked patch (V_{out}), and the rate of creep on the "locked" patch (V_{creep}).

[128] In the model, the soon-to-fail 1935 patch is slipping aseismically at more than half of the plate rate and the interface farther outboard is slipping at a rate slightly higher than the plate rate. The solution is tightly constrained by the observed peak emergence at Mm and Lg. For example, if we fully lock the shallow (red and orange) patches, the predicted peak emergence value will increase to about 7.5 mm/yr, greatly overestimating the observed values. Moreover, the slope and magnitude of the submergence trough between Mm and Tb places tight constraints on the amount and proportion of aseismic slip on the red and the orange patches. A model using a 1 mm/yr correction for the global sea level rise gives a similar solution but the amount of slip on the orange and the red patches increases by about 20% [*Natawidjaja*, 2003].

2.6.3.2. Modeling of Deformation Rates for the Period From 1935 to 1961

[129] The location of the hingeline separating domains of emergence and submergence in the post-1935 period differs no more than 5 km from that of the pre-1935 deformation (cf. Figures 15a and 15c). Therefore we felt justified in starting our model iterations with the same initial condition, namely that the updip edge of the fully creeping dislocation be fixed at 27 km depth, nearly beneath the hingeline. Using this constraint, however, the model could not achieve a good fit to the emergence rate at either Masin (Ms) or Memong (Mm) [*Natawidjaja*, 2003]. An alternate model, in which the updip tip of the fully creeping dislocation is 10 km farther updip or about 116 km from the trench, fits both points much better (Figure 19, panel C).

[130] Our model also suggests that following the 1935 event the shallow part of the interface continued slipping at about the same rate as before 1935 and extended downdip well into the upper part of the 1935 rupture (Figure 19c). The central portion of the 1935 patch, however, appears to have completely locked up.

2.6.3.3. Modeling of Deformation Rates for the Period 1962–2000

[131] Since the deformation rates of the past forty years around Tanabala and Tanamasa do not vary much along strike, we can justify using a 2-D inversion. However, we exclude the two points from the reefs of Pini Island (i.e., Masin and Lambak sites), since these data clearly reflect some other process. We tried several model scenarios. If we lock the entire interface between the trench and a point 135 km downdip, the model fits the paleogeodetic data well, but grossly exceeds the low submergence rate at the westernmost point (Tb). Our data at Tb are very good; therefore this fully locked scenario is unacceptable. To produce a better fit to this data point, we must allow some slip on the 1935 patch and on the patch farther outboard (Figure 19f). In this model the downdip limit of the locked patch is quite stable at 27 km depth, 125 km downdip from the trench (the lower limit of the 1935 rupture).

[132] A comparison with the best fitting models for the previous period, 1935–1961, shows only one principal difference in behavior between the two periods (cf. Figure 19, panels C and F). Before 1962 the outboard patch was slipping at a rate near or slightly in excess of the plate rate. After 1962, the rate on the outboard interface dropped

to only about half the plate rate, but extended about 10 km further downdip.

3. Discussion and Conclusions

[133] We have investigated a century of vertical deformations of the hanging wall block of the Sumatran subduction zone near the equator. Microatolls from 16 sites there record sea level time series that span the twentieth century and include deformation associated with the M_w 7.7 earthquake in 1935.

[134] The paleogeodetic records reveal three distinct, long periods of aseismic deformation separated by the 1935 earthquake and two rapid aseismic events in 1962. The pattern of coseismic vertical deformation in 1935 is the standard pattern for a shallow subduction event, with about 2.3 m of slip on a 35-km-wide, 60-km-long patch causing uplift nearer the trench and subsidence farther landward (Figure 19, panel B). Source parameters derived from the paleogeodetic data are consistent with those derived from seismological data, although the magnitude of slip calculated from the paleogeodetic data is slightly greater (Figure 17).

[135] The pattern of rapid submergence in 1962 suggests rapid aseismic failure of the deepest strip of the coseismic 1935 patch and of the section of the interface updip from the 1935 patch.

[136] Our coral records show clearly that interseismic deformation rates and patterns during the decades before, between and after the 1935 and 1962 events varied markedly (Figure 15). Simple elastic dislocation models of the subduction interface provide plausible interpretations of how slip on the subduction interface differed between these periods. Before the 1935 earthquake, slip outboard of the 1935 rupture patch appears to have been occurring at about 5.5 cm/yr, a rate somewhat greater than the orthogonal component of the plate rate (Figure 19a). Moreover, the soon-to-rupture 1935 patch was slipping at about 2.5 cm/yr.

[137] In the quarter century after the 1935 earthquake, the center of the 1935 patch appears to have been completely locked. However, the lower portion of the 1935 patch was slipping along with deeper parts of the interface at the orthogonal component of the plate rate (Figure 19, panel C). Furthermore, the upper portion of the 1935 patch was slipping along with the shallowest section of the interface at a rate of about 5.3 cm/yr. Thus it appears that after the 1935 rupture, the upper and lower thirds of the 1935 seismic patch experienced afterslip at about the same rates as aseismic slip was occurring on the updip and downdip sections of the subduction interface.

[138] The modeling suggests that this behavior of the interface changed abruptly after the rapid aseismic episode of 1962. In the 40 years since 1962, the entire interface has been slipping. The slip rate of the shallow interface, however, has slowed to about 2.7 cm/yr, about half the plate rate, and includes the upper two thirds of the 1935 rupture patch (Figure 19, panel F). The remainder of the 1935 patch, between about 112 and 125 km downdip from the trench, has been slipping at the low rate of about a cm/yr.

[139] What is the significance of these data and models? The data demonstrate that the behavior of the subduction interface above a depth of about 30 km has varied markedly
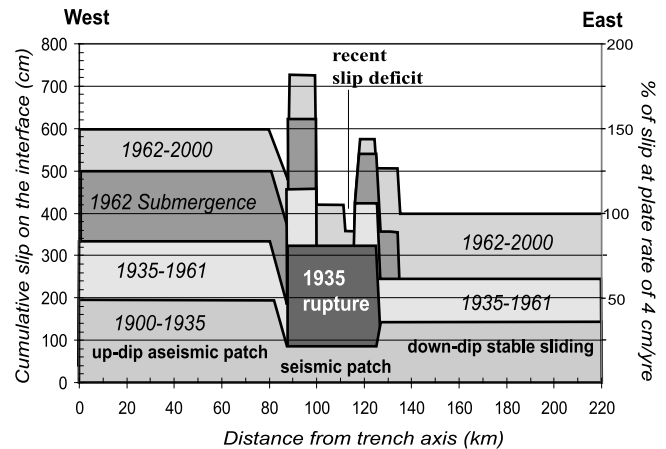

Figure 20. Seismic and aseismic slip history on the subduction interface from 1900 to 2000 based on paleogeodetic data and elastic dislocation models. The dark, shaded areas represent the amount of slips in the 1935 and 1962 submergence events respectively. The lighter shaded areas represent aseismic slips during intervening periods. Note that the 1962 emergence is excluded in the figure because of its ambiguity.

in time and space (Figure 19). The elastic models are simply a first attempt to quantify that behavior. They suggest that individual locations on the interface changed their behavior after the 1935 and 1962 events. Furthermore, locations that ruptured seismically in 1935 appear to have slipped aseismically during other events and periods. What does this variability reveal about the nature of subduction processes, not only in western Sumatra but more generally as well?

3.1. Expenditure of the Subduction Slip Budget Throughout the Twentieth Century

[140] Recent GPS geodetic measurements show that, by and large, decadal rates of strain accumulation across entire plate boundaries do not differ from plate rates averaged over a million years or so [Gordon et al., 1990; Larson et al., 1997, 1999; Royer et al., 1997]. Thus rates of strain accumulation across entire plate boundaries do not appear to vary over a broad range of time scales.

[141] However, strain accumulation equals strain relief only if a fault's decadal slip rate accommodates all the strain accumulated during the decade (e.g., as along the central, creeping reach of the San Andreas fault [Lisowski and Prescott, 1981]). It is well established that most faults do not balance their accounts this frequently. Periods of strain accumulation without rupture may continue for centuries or millennia, with strains being relieved by slip that occurs in just seconds to days. These centennial and millennial imbalances between strain accumulation and relief within plate boundary regions are poorly understood, because data on serial fault rupture and strain accumulation over centuries and millennia are sparse.

[142] The data we have obtained allow us to gain an increment of insight into this matter. Figure 20 shows a twentieth century slip budget for the Sumatran subduction

interface, based upon the elastic modeling of the previous section. Along the x axis is the distance downdip from the trench, and along the left y axis is slip that accumulated during the twentieth century, according to the models in Figure 19. Faster slip events appear as darker shaded areas, and periods of slower slip appear as lighter shaded areas. The right-hand y axis shows the status of the interface relative to the slip that would have accumulated at the long-term plate rate. For example, the deeper part of the interface, more than about 130 km from the trench, experienced 100% of this amount, because we fixed its rate of slip at the long-term rate of 4 cm/yr.

[143] The salient points of this display are these: The updip, shallow parts of the subduction interface have slipped about 50% more than would have been produced by a century of slip at the plate rate. Note that, using 1 mm/yr rather than 2 mm/yr correction for the global sea level rise in the modeling will make the predicted slip rate 25% greater or more; thus a century of total slip on this shallow interface will be about 75% or more than that at the plate rate. A large fraction of this slip occurred during the rapid 1962 submergence event. Had this event not occurred, the cumulative slip for the century would have nearly equaled the 4 m that would accumulate at the plate rate. The upper and lower thirds of the patch that failed seismically in 1935 also experienced an amount of slip in excess of 4 m. Well over half of the slip on these sections accumulated during the 1935 and 1962 events. Only the central third of the 1935 patch exhibited about the amount of slip that would have accrued at the plate rate. A little over half of this occurred during the 1935 event; the remainder accumulated slowly in the decades before 1935 and after 1962.

[144] To balance the excess of twentieth century slip along the shallowest section of the interface, the rate of slip must be lower during a prior or later period. During the first six decades of the century, the shallow section of the interface accumulated about 90 cm more slip than would have been required to accommodate plate convergence. In the 1962 event, this interface slipped about 160 cm. Thus, from 1900 to 1962, the slip accumulated in excess of what would have accumulated at the plate rate is 250 cm. Thus it is reasonable to hypothesize that in the period 1900–1962 the interface relieved strains that had accumulated at the plate rate during at least the prior 60 years (i.e., 250/4 years). This estimate of accumulation time would increase by a factor of 3 (4/(4−2.7)), to about 180 years, if one assumes that the shallow interface was creeping at its current rate of 2.7 cm/yr prior to the twentieth century. These calculations suggest that the rapid creep episode of 1962 need not repeat very often to alleviate strain accumulation, perhaps only every other century or so. It also seems likely that lengthy periods of excess slip, as occurred in the decades prior to and following the 1935 event, are rare. Perhaps these occur only in the decades immediately before and after slip on the 1935 seismic patch.

[145] The slip deficit that accumulated on the 1935 patch in the 35 years prior to the earthquake was about 50 cm, because the patch was slipping at 2.5 cm/year, that is, 1.5 cm/yr slower than the plate rate. In 1962, after a 27-year hiatus, this patch slipped on its updip and downdip edges. Since then, the 1935 patch appears to have resumed slipping slowly at a rate similar to that prior to 1935. If strains

accumulate during interseismic periods at about the current rate of 1.5 cm/yr, 150 years or so would be required to accumulate strains that could result in 2.3 m of seismic slip. This crude estimate of recurrence is quite consistent with the length of the period between 1935 and AD 1797, the date of the previous rupture of the 1935 patch [*Natawidjaja*, 2003].

[146] The greatest excesses of twentieth century slip are on the upper edge of the 1935 rupture patch. This section experienced slip during both the 1935 and 1962 events and creep in the adjoining periods. The fact that these excess slips are on the edges of the 1935 rupture suggests that they are the products of stress concentrations produced by the 1935 rupture.

[147] One general implication of our data and initial 2-D modeling is that the ratio of aseismic to seismic slip on subduction interfaces varies downdip as well as along-strike and varies with time as well. The fraction of aseismic slip from the trench to 90 km downdip or so is about 1.0, and aseismic slip during the twentieth century has been higher than the plate convergence rate. The ratio also appears to be 1.0 farther downdip than about 130 km. The fraction of aseismic slip on the 1935 patch averages about 0.4, but the values are much higher on the upper and lower thirds of the patch and much lower within the central third.

3.2. Implication of Paleogeodetic Behavior for Rheology of the Subduction Interface

[148] Previous studies have shown that the rheology of a subduction interface is strongly controlled by temperature, fluid pressures and mineralogical assemblages [e.g., *Hyndman et al.*, 1995; *Oleskevich et al.*, 1999]. These factors, in general, divide the subduction interface into three major zones: an upper slow-slip zone, a middle locked, seismic zone, and a lower stable-sliding zone [*Hyndman and Wang*, 1995; *Kodaira et al.*, 2002; *Oleskevich et al.*, 1999]. This division seems to explain adequately many observations from other subduction zones [e.g., *Dragert et al.*, 1994; *Freymueller et al.*, 2000; *Hyndman and Wang*, 1995; *Kanamori*, 1973; *Kodaira et al.*, 2002; *Oleskevich et al.*, 1999; *Thatcher*, 1984a].

[149] Modeling of our paleogeodetic data suggests that these major mechanical boundaries of the interface are present in Sumatra, as well, but that neither their boundaries nor their behavior are stationary over decades to centuries. The modeling suggests that slip rates on the shallow aseismic patch may vary by a factor of two throughout the earthquake cycle (compare Figure 19, panels A, C, and F) and may even experience rapid aseismic events (Figure 19, panel E). Furthermore, the edges of the "locked" patch may slip aseismically in the decades before and after seismic rupture. Even the central part of a seismic patch appears to have experienced steady aseismic slip during the decades prior to seismic failure (Figure 19, panel A). These changes in behavior of the interface contradict simple notions that fault behavior is invariant, with permanent boundaries between stable and unstable sliding [e.g., *Pacheco et al.*, 1993; *Thatcher*, 1984a].

[150] Our modeling does support the existence of a shallow, aseismic interface. Although it seems to have experienced variable rates of stable sliding and even one rapid bursts of aseismic slip, the shallowest part of the interface, from the trench to about 90 km downdip (~15 km depth), has been

slipping only aseismically throughout the twentieth century. This upper section, then, appears to represent a wholly aseismic zone, such as postulated in many subduction models [*Kasahara et al.*, 2001; *Kodaira et al.*, 2002; *Moore and Saffer*, 2001; *Oleskevich et al.*, 1999].

[151] What structure or rheology controls the downdip edge of the 1935 seismic patch? Our modeling constrains tightly the downdip edge of the 1935 rupture to a depth of about 25 km. With the possible, but tenuous, exception of deep slip during the 1962 emergence event (Figure 19, panel D), no seismic or rapid aseismic episode appears to have occurred farther downdip during the century.

[152] Seismic refraction surveys in the forearc basin around Nias Island, just north of the equator, reveal that the continental Moho is about 25 km deep [*Kieckhefer et al.*, 1980]. More recent seismic reflection surveys offshore of southern Sumatra also found the Moho to be at this depth [*Kopp et al.*, 2001]. Thus it appears that the downdip edge of the seismogenic patch corresponds to the base of the crust and that slip between the downgoing slab and the upper mantle is wholly by stable, aseismic sliding.

[153] In summary, our paleogeodetic model largely agrees with a general subduction model that postulates three major divisions of the subduction interface characterized by different mechanical behaviors. Our model suggests, however, that the boundaries of these zones are not stationary over decades or centuries.

[154] We have not yet tried to incorporate visco-elastic phenomena, such as mantle relaxation, into our model. However, the fact that linear regressions fit most of the HLS time series in the periods between the 1935 and 1962 events strongly suggests that rates of deformation in the intervening decades are not dependent on the time since perturbation by the seismic rupture of 1935 and the rapid aseismic events of 1962. Thus the presence of viscous materials at the interface and the readjustment of the upper mantle appear to have negligible effects.

References

Abercrombie, R. E., M. Antolik, and G. Ekström (2003), The June 2000 M_w 7.9 earthquakes south of Sumatra: Deformation in the India-Australia Plate, *J. Geophys. Res.*, *108*(B1), 2018, doi:10.1029/2001JB000674.

Ando, M. (1975), Source mechanisms and tectonic significance of historical earthquakes along the Nankai through, Japan, *Tectonophysics*, *27*, 119–140.

Atwater, B. (1992), Geologic evidence for earthquakes during the past 2000 years along the Copalis River, southern coastal Washington, *J. Geophys. Res.*, *97*, 1901–1919.

Barnett, T. P. (1984), The estimation of global sea level change: A problem of uniqueness, *J. Geophys. Res.*, *89*, 7980–7988.

Berlage, H. P., Jr. (1936), Aardbevingen, *Natuurk. Tijdschr. Ned.*, 191–192.

Budhitrisna, T., and S. Andi Mangga (1990), Geologi Lembar Pagai dan Sipora Sumatra (Geology of the Pagai and Sipora Quadrangle, Sumatra), Indonesian Geol. Res. and Dev. Cent., Bandung.

Cheng, H., R. L. Edwards, J. Hoff, C. D. Gallup, D. A. Richards, and Y. Asmerom (2000), The half-life of uranium-234 and thorium-230, *Chem. Geol.*, *169*, 17–33.

Deplus, C., M. Diament, H. Hebert, G. Bertrand, S. Dominguez, J. Dubois, J. Malod, P. Patriat, B. Pontoise, and J. Sibilla (1998), Direct evidence of active deformation in the eastern Indian oceanic plate, *Geology*, *26*, 131–134.

Dragert, H., R. D. Hyndman, G. C. Rogers, and K. Wang (1994), Current deformation and the width of the seismogenic zone of the northern Cascadia subduction thrust, *J. Geophys.Res.*, *99*, 638–668.

Dragert, H., K. L. Wang, and T. S. James (2001), A silent slip event on the deeper Cascadia subduction interface, *Science*, *292*, 1525–1528.

Edwards, R. L., J. H. Chen, and G. J. Wasserburg (1987), 238U, 234U, 230Th, 232Th systematics and the precise measurement of time over the past 500,000 years, *Earth Planet. Sci. Lett.*, *81*, 175–192.

Engdahl, E., R. van der Hilst, and R. Buland (1998), Global teleseismic earthquake relocation with improved travel times and procedures for depth determination, *Seismol. Soc. Am. Bull.*, *88*, 722–743.

Fitch, T. (1972), Plate convergence, transcurrent faults, and internal deformation adjacent to southeast Asia and the western Pacific, *J. Geophys. Res.*, *77*, 4432–4462.

Freymueller, J. T., S. C. Cohen, and H. J. Fletcher (2000), Spatial variations in present-day motion, Kenai Peninsula, Alaska, and their implications, *J. Geophys. Res.*, *105*, 8079–8101.

Gordon, R., C. DeMets, and D. Argus (1990), Kinematic constraints on distributed lithospheric deformation in the equatorial Indian Ocean from present motion between the Australian and Indian plates, *Tectonics*, *9*(3), 409–422.

Gornitz, V., S. Lebedeff, and J. Hansen (1982), Global sea level trend in the past century, *Science*, *215*, 1611–1614.

Heki, K., H. Miyazaki, and H. Tsuji (1997), Silent fault slip following an interplate earthquake at the Japan trench, *Nature*, *386*, 595–598.

Hyndman, R. D., and K. Wang (1995), The rupture zone of Cascadia great earthquakes from current deformation and the thermal regime, *J. Geophys. Res.*, *100*, 2133–2154.

Hyndman, R. D., K. Wang, and M. Yamano (1995), Thermal constraints on the seismogenic portion of the southwestern Japan subduction thrust, *J. Geophys. Res.*, *100*, 15,373–15,392.

Indrawadi, and Y. Efendi (2000), Kasus red tide di perairan Sumatera Barat, paper presented at Lokakarya Pengelolaan dan Iptek Terumbu Karang Indonesia, COREMAP, Bali, Indonesia.

Kanamori, H. (1973), Mode of strain release associated with major earthquakes in Japan, *Annu. Rev. Earth Planet. Sci.*, *1*, 213–239.

Kanamori, H., and D. L. Anderson (1975), Theoretical basis of some empirical relations in seismology, *Seismol. Soc. Am. Bull.*, *65*, 1073–1095.

Kasahara, J., A. Kamimura, G. Fujie, and R. Hino (2001), Influence of water on earthquake generation along subduction zones, *Bull. Earthquake Res. Inst. Univ. Tokyo*, *76*(3), 291–304.

Katili, J. A., and F. Hehuwat (1967), On the occurrence of large transcurrent faults in Sumatra, Indonesia, *J. Geosci. Osaka City Univ.*, *10*, 5–17.

Kieckhefer, R. M., G. G. Shor Jr., and J. R. Curray (1980), Seismic refraction studies of the Sunda trench and forearc basin, *J. Geophys. Res.*, *85*, 863–889.

Knutson, D. W., and S. V. Smith (1972), Coral chronometers: Seasonal growth bands in reef corals, *Science*, *177*, 270–272.

Kodaira, S., E. Kurashimo, J. O. Park, N. Tkahashi, A. Nakanishi, S. Miura, T. Iwasaki, N. Hirata, K. Ito, and Y. Kaneda (2002), Structural factors controlling the rupture process of a megathrust earthquake at the Nankai trough seismogenic zone, *Geophys. J. Int.*, *149*, 815–835.

Kopp, H., E. R. Flueh, D. Klaeschen, J. Bialas, and C. Reichert (2001), Crustal structure of the central Sunda margin at the onset of oblique subduction, *Geophys. J. Int.*, *147*, 449–474.

Larson, K., J. Freymueller, and S. Philipsen (1997), Global plate velocities from the Global Positioning System, *J. Geophys. Res.*, *102*, 9961–9981.

Larson, K. M., R. Burgmann, R. Bilham, and J. T. Freymueller (1999), Kinematics of the India-Eurasia collision zone from GPS measurements, *J. Geophys. Res.*, *104*, 1077–1094.

Lisowski, M., and W. H. Prescott (1981), Short-range distance measurements along the San-Andreas fault system in central California, 1975 to 1979, *Seismol. Soc. Am. Bull.*, *71*(5), 1607–1624.

Lowry, A. R., K. M. Larson, V. Kostoglodov, and R. Bilham (2001), Transient fault slip in Guerrero, southern Mexico, *Geophys. Res. Lett.*, *28*, 3753–3756.

McCaffrey, R. (1991), Slip vectors and stretching of the Sumatran fore arc, *Geology*, 19, 881–884.

Miller, M. M., T. Melbourne, and D. J. Johnson (2002), Periodic slow earthquake from the Cascadia subduction zone, *Science*, 295, 2423.

Moore, J. C., and D. Saffer (2001), Updip limit of the seismogenic zone beneath the accretionary prism of southwest Japan: An effect of diagenetic to low-grade metamorphic processes and increasing effective stress, *Geol. Soc. Am. Bull.*, 29, 183–186.

Natawidjaja, D. H. (2003), Neotectonics of the Sumatran Fault and paleogeodesy of the Sumatran subduction zone, Ph.D. thesis, Calif. Inst. of Technol., Pasadena.

Newcomb, K. R., and W. R. McCann (1987), Seismic history and seismotectonics of the Sunda Arc, *J. Geophys. Res.*, 92, 421–439.

Oleskevich, D. A., R. D. Hyndman, and K. Wang (1999), The updip and downdip limits to great subduction earthquakes: Thermal and structural models of Cascadia, south Alaska, SW Japan, and Chile, *J. Geophys. Res.*, 104, 14,965–14,991.

Pacheco, J. F., R. S. Lynn, and C. H. Scholz (1993), Nature of seismic coupling along simple plate boundaries of the subduction type, *J. Geophys. Res.*, 98, 14,133–14,159.

Peltier, W., and A. Tushingham (1989), Global sea level rise and the greenhouse effect: Might they be connected, *Science*, 244, 806–810.

Peltier, W. R., and A. M. Tushingham (1991), Influence of glacial isostatic adjustment on tide gauge measurements of secular sea level change, *J. Geophys. Res.*, 96, 6779–6796.

Plafker, G. (1965), Tectonic deformation associated with the 1964 Alaskan earthquake, *Science*, 148, 1675–1687.

Prawirodirdjo, L. (2000), A geodetic study of Sumatra and the Indonesian region: Kinematics and crustal deformation from GPS and triangulation, Ph.D. dissertation, Univ. of Calif., San Diego.

Prawirodirdjo, L., et al. (1997), Geodetic observations of interseismic strain segmentation at the Sumatra subduction zone, *Geophys. Res. Lett.*, 24, 2601–2604.

Prawirodirdjo, L., Y. Bock, J. Genrich, S. S. O. Puntodewo, J. Rais, C. Subarya, and S. Sutisna (2000), One century of tectonic deformation along the Sumatran fault from triangulation and Global Positioning System surveys, *J. Geophys. Res.*, 105, 6779–6796.

Rivera, L., K. Sieh, D. Helmberger, and D. H. Natawidjaja (2002), A comparative study of the Sumatran subduction-zone earthquakes of 1935 and 1984, *Seismol. Soc. Am. Bull.*, 92, 1721–1736.

Royer, J., R. Gordon, C. DeMets, and P. Vogt (1997), New limits on the motion between India and Australia since chron 5 (11 Ma) and implications for lithospheric deformation in the equatorial Indian Ocean, *Geophys. J. Int.*, 129(1), 41–74.

Saji, N. H., B. N. Goswami, P. N. Vinayachandran, and T. Yamagata (1999), A dipole mode in the tropical Indian ocean, *Nature*, 401, 360–363.

Savage, J. (1983), A dislocation model of strain accumulation and release at a subduction zone, *J. Geophys. Res.*, 88, 4984–4996.

Savage, J. C. (1995), Interseismic uplift at the Nankai subduction zone, southwest Japan, 1951–1990, *J. Geophys. Res.*, 100, 6339–6350.

Savage, J. C., and G. Plafker (1991), Tide-gauge measurements of uplift along the south coast of Alaska, *J. Geophys. Res.*, 96, 4325–4335.

Scoffin, T. P., and D. R. Stoddart (1978), The nature and significance of microatolls, *Philos. Trans. R. Soc. London, Ser. B*, 284, 99–122.

Sieh, K. (1996), The repetition of large-earthquake ruptures, *Proc. Natl. Acad. Sci.*, 93(9), 3764–3771.

Sieh, K., and D. Natawidjaja (2000), Neotectonics of the Sumatran fault, Indonesia, *J. Geophys. Res.*, 105, 28,295–28,326.

Sieh, K., M. Stuiver, and D. Brillinger (1989), A more precise chronology of earthquakes produced by the San Andreas fault in southern California, *J. Geophys. Res.*, 94, 603–623.

Sieh, K., S. N. Ward, D. H. Natawidjaja, and B. W. Suwargadi (1999), Crustal deformation at the Sumatran subduction zone, *Geophys. Res. Lett.*, 26, 3141–3144.

Sieh, K., D. Natawidjaja, S. Ward, R. Edwards, B. Suwargadi, and J. Zachariasen (2000), Paleogeodetic and paleoseismologic constraints on the earthquake cycle of the Sumatran subduction zone, in *Hokudan International Symposium and School on Active Faulting*, edited by K. T. K. Okumura and H. Goto, pp. 459-463, Letter Press, Hokudan, Japan.

Smithers, S. G., and C. D. Woodroffe (2000), Microatolls as sea-level indicators on a mid-ocean atoll, *Mar. Geol.*, 168, 61–78.

Taylor, F. W., J. Frohlich, J. Lecolle, and M. Strecker (1987), Analysis of partially emerged corals and reef terraces in the central Vanuatu arc: Comparison of contemporary coseismic and nonseismic with Quaternary vertical movements, *J. Geophys. Res.*, 92, 4905–4933.

Thatcher, W. (1984a), The earthquake deformation cycle at the Nankai through, southwest Japan, *J. Geophys. Res.*, 89, 3087–3101.

Thatcher, W. (1984b), The earthquake deformation cycle, recurrence, and the time-predictable model, *J. Geophys. Res.*, 89, 5674–5680.

Thatcher, W. (1989), Earthquake recurrence and risk assessment in circum-Pacific seismic gaps, *Nature*, 341, 432–434.

Woodroffe, C., and R. McLean (1990), Microatolls and recent sea level change on coral atolls, *Nature*, 344, 531–534.

Zachariasen, J. (1998), Paleoseismology and paleogeodesy of the Sumatran Subduction Zone: A study of vertical deformation using coral microatolls, dissertation thesis, Calif. Inst. of Technol., Pasadena.

Zachariasen, J., K. Sieh, F. W. Taylor, R. L. Edwards, and W. S. Hantoro (1999), Submergence and uplift associated with the giant 1833 Sumatran subduction earthquake: Evidence from coral microatolls, *J. Geophys. Res.*, 104, 895–919.

Zachariasen, J., K. Sieh, F. W. Taylor, and W. S. Hantoro (2000), Modern vertical deformation above the Sumatran subduction zone: Paleogeodetic insights from coral microatolls, *Seismol. Soc. Am. Bull.*, 90(4), 897–913.

————————

H. Cheng and R. L. Edwards, Department of Geology and Geophysics, University of Minnesota, 310 Pillsbury Drive, SE, Minneapolis, MN 55455, USA.

G. Galetzka and K. Sieh, Division of Geological and Planetary Sciences, California Institute of Technology, Mail Stop 100-23, 1200 East California Boulevard, Pasadena, CA 91125, USA.

D. H. Natawidjaja and B. W. Suwargadi, Research Center for Geotechnology, Indonesian Institute of Sciences, Komplek LIPI Gd. 70, J1. Sangkuriang, Bandung 40135, Indonesia. (danny@gps.caltech.edu)

S. N. Ward, Institute of Geophysics and Planetary Physics, University of California, Santa Cruz, CA 95064, USA.